EXPERIMENTS WITH A NOVEL CCD POLARIMETER

By

Dirk Neumayer

SUBMITTED TO THE
DEPARTMENT OF PHYSICS AND ASTRONOMY
FOR
THE DEGREE OF
MASTER OF SCIENCE
AT
UNIVERSITY OF GLASGOW
GLASGOW G12 8QQ
SCOTLAND, UK
SEPTEMBER 2000

♡

To Nadine and the Stars.

Summary

Until recently, photo electric devices have mostly been used in stellar polarimetry. They usually involve a rotatable modulator, such as either a polaroid or a half-waveplate with fixed polaroid in the beam of light. This modulator is either positioned at different angles and exposures are taken (at least 3 exposures at different positions are necessary, to compute the normalized Stokes parameters q and u) or it is rotated continuously. The second method has the advantage, that fluctuations in sky-transparency are averaged out. But a major drawback of photo electric devices is that they are essentially single pixel devices, so that only one object at a time can be observed. Another handicap are dead-time problems. If bright objects are to be observed, neutral density filters have to be used to reduce the photon flux to acceptable counting rates which is rather painful since it is the number of counted photons that determines the final accuracy.

With the advent of CCD technology these detectors are now more and more applied in stellar polarimetry. CCDs, being imaging devices, allow the observation of whole sky areas or several objects at a time. The method which is usually applied involves taking several exposures with a modulator at different angles. Once again, changes in sky transparency have to be taken into account. Also the total photon count per exposure is limited, this time by the full-well capacity of the pixels and the number of pixels used.

In this Thesis a new design for a CCD-Polarimeter is presented which is a hybrid between the traditional photo electric instruments and modern CCD-imaging. Analogous to photomultiplier devices, the modulator is rotated continuously. A co-rotating glass wedge in the light path deviates the beam and the eventual image is recorded

by a CCD camera. The rotation together with the deviation converts the point-like images of the stars into rings. These rings contain, encoded as intensity modulation along their circumference, all the information necessary to determine the normalized Stokes parameters. By choosing suitable deviation angles, either a group of stars can be observed simultaneously, or a single star, slightly out of focus, can be observed with high accuracy, since a high photon count can be achieved by spreading the light into many pixels along the ring. Theoretically with the presented instrument an accuracy for p of about $\pm 7 \times 10^{-5}$ could be achieved with one single exposure. Variations in sky transparency do not cause any problems since they are averaged out.

This design has been explored by means of a simple prototype and new data reduction techniques have been developed to reduce and analyze the obtained data. In particular, finding the circles and extracting the information from the intensity modulation along the circumference of the circle.

Experiments with the prototype have been carried out, both in the laboratory using artificial 'stars' and at the Cochno observatory, this time involving real stars. Different modulators and deviators have been tested. During the tests various problems were encountered, the instrument was returned to the workshop and modifications were made. This cycle of testing and improving was quite time consuming and the main problem, the motor inducing vibrations and not rotating uniformly could not really be overcome in the current design. The obtained frames were used to check the data reduction and analyzing software. The presented algorithms fulfilled their tasks satisfactorily.

The experiments with the prototype CCD-Polarimeter have shown that in principle it is a very potent technique but with some, mostly mechanical, obstacles to overcome. Based on the experiences in the described test runs, improvements for a further second prototype are proposed.

It is self evident that this Thesis has been prepared using LaTeX 2_ε and its appropriate packages. One of the niceties of this is the possibility of inventing special fonts. It turns out that the stellar images containing the polarimetric information are so beautiful in concept and appearance that it was impossible to resist making one special character which has been incorporated in the title page.

"In some ways this single letter "◌" sums up the ingenuity of mankind of being able to express and write about ideas of the Universe simply by using star light."

David Clarke, 2000.

Table of Contents

List of Tables

List of Figures

Acknowledgments

It is a pleasure to thank Dr. David Clarke for all his support, guidance, patience with both myself and the instrument and his coruscating wit. Being with him was very inspiring, refreshing and made this research project an enjoyable experience.

I am indebted to Colin Hunter for his efforts in the workshop and bringing the instrument back and forth to the Cochno observatory.

Thanks are due to Prof. John Brown for being an excellent host and to the Astronomy Group for being a diverse collection of wonderful people. Special thanks to Graeme Stewart and Norman Gray for their help in programming.

Further I wish to thank Dr. David Clarke, Nadine Häring and Stephen Webster for helpful discussions and reading the manuscript.

In addition I would like to express my thanks to my parents for their support.

Many free available marvelous electronic tools were used for typesetting the Thesis, creating the figures and analyzing the data. Their creators all have my humble thanks.

1

Introduction

In the words of a one-time popular song: "Birds do it, Bees do it...". In the animal kingdom many species are able to do it. In fact, much research is carried out on the sensitivity to it of practically all living creatures. For example as recently as 1999, it has been found that spiders use it to find their way home after dawn [Dacke et al., 1999]. Light has an additional property to its well known characteristics like colour and intensity, viz: *polarization*. It is this characteristic that animals put to advantage in determining direction — it is not available to humans as our retinas are virtually insensitive to polarization.

To allow us to sense and measure this property of polarization, we need special optical devices. The topic of this Thesis is the building and evaluating of such a device, in this case a device to analyze stellar light.

But what is polarization? Light can be represented as transverse electromagnetic waves made up of mutually perpendicular, fluctuating electric and magnetic fields. In a beam of light where all electric field vectors $\vec{E}$ have the same direction of vibration, we speak of linearly polarized light. A single wave train, emitted by an excited atom is an example for linear polarized light. Natural or unpolarized light, however, consists of the total output from a very large number of randomly oriented atomic emitters.

The average of the directions of all the electric field vectors, sampled over a few cycles of the wave is zero. There are several processes that give rise to polarization. A few that are of special interest in stellar polarimetry are as follows:

- **Thomson scattering** (scattering by free electrons), e.g. solar corona, envelopes of early-type stars
- **Mie scattering** (scattering by small grains), e.g. comets, reflection nebulae, atmosphere of late-type stars, circumstellar discs, interstellar polarization
- **Rayleigh scattering** (scattering by molecules), e.g. terrestrial blue sky, late-type stellar atmospheres
- **Hanle effect**, due to resonance scattering of bound electrons in magnetic fields, e.g. in emission lines of solar chromosphere and corona.

Stellar polarimetry is a useful diagnostic for learning about stars and the interstellar material (ISM).

As an example of a recent and exciting application, polarimetry is being applied to identifying possible planetary systems and circumstellar disks in nearby stars. [Rivera and Penprase, 1999]. It is hoped to detect the thinned disks around main-sequence stars by observing the polarization of light reflecting off the top of the disk at a shallow angle.

1.1 A brief historical outline

The concept of polarization as an additional property of light emerged in 1808. Etienne-Louis Malus, lying ill in a hospital, discovered a phenomenon, later to be named *polarization.* He was looking through a calcite crystal at the light reflected obliquely from a

window of the Luxembourg Palace in Paris, and observed that the two images produced by the calcite were extinguished alternately when he rotated the crystal [see Geherls, 1974, page 5]. His observation linked the property within reflected light with the same property within the separate beams produced by calcite crystals. Malus is also famous for the discovery of the $\cos^2\theta$ law associated with the flux of light transmitted by two polarizers, set with their principal axes at an angle θ with respect to each other [see Malus, 1810].

Immediate investigations by Arago followed to see if astronomical objects exhibit polarized light. The moon and comets were observed, but star light could not be measured, due to limitations set by the human eye.

In 1852 Sir George G. Stokes introduced the four parameters, named after him [Stokes, 1852], which can be used to describe partially polarized light (see Appendix A for a mathematical description).

Although photography was developed early in the 19th century, there was a major delay in its application to polarimetry of stellar sources. The first reference related to its use is Öhman [1934] but only limited advances were made.

A main boost to stellar polarimetry was triggered by the development of photomultiplier tubes (first applied by Hall [1948]) following the theoretical predictions by Chandrasekhar [1946]. In this latter paper Chandrasekhar predicted that the radiation of early-type stars is polarized and varying from zero at the center of the disk to 11 % at the limb and that this intrinsic polarization *"could be detected under suitably favorable conditions"*.

A short time later Hall and Mikesell [1949] and Hiltner [1949] investigated Chandrasekhars predictions by monitoring eclipsing binary systems but, by serendipity, they discovered interstellar polarization instead. Figure 1.1 on the following page shows some of the findings of Hall and Mikesell [1949].

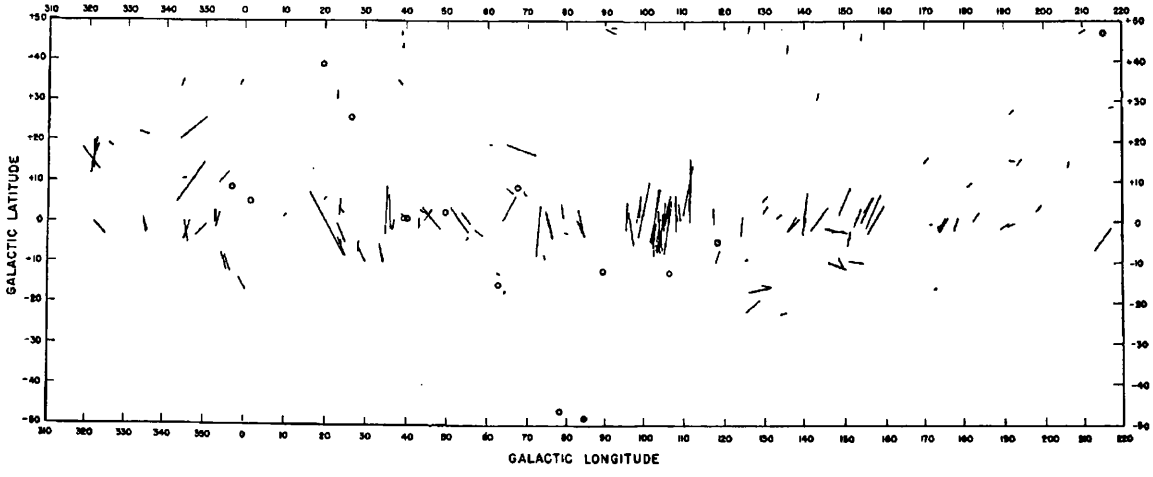

Fig. 1.1. Vector diagram showing polarization of individual stars [Hall and Mikesell, 1949]. Note that the directions of vibration are generally orthogonal to the Galactic plane.

From these observations Hall and Mikesell concluded: *"Several groups of stars show considerable homogeneity (see Fig. 1.1) in the direction of their planes of polarization; this suggests that their light has passed through the same polarizing cloud or clouds."* Independent of these observations, Hiltner discovered the same phenomena. In his paper [Hiltner, 1949] he concludes: *"Furthermore, it is obvious that this polarization is not associated with the individual stars but is introduced to stellar radiation in its passage through interstellar space"*. Also *"if the polarization is a consequence of scattering by interstellar particles, it follows that these particles must be unsymmetrical, that is, elongated, and that these particles are subject to some alignment force. This force may take the form of magnetic fields"*.

Following the discovery of interstellar polarization, observations were pursued to investigate the properties of the Galactic magnetic field and the interstellar material (ISM). Davis and Greenstein [1951] proposed that the observed parallelism of the directions of polarization of different stars is due to small elongated dust grains, that

are aligned by a Galactic magnetic field. In their paper properties of such grains are discussed, e.g. size, shape, composition and dielectricity. They presented an alignment model which is now known as the 'Davis-Greenstein mechanism'. It explains the alignment of rapidly spinning grains by a torque due to paramagnetic relaxation in material containing a few percent of iron. Vast developments have been made in the study of the ISM since then. Especially with new instruments that are capable to measure in the infrared, like the ground-based telescope UKIRT or the astronomical satellites IRAS and ISO, a great deal has been learned about the nature of the interstellar dust.

In the era of 50 years ago, most stellar polarimetry was undertaken using photo electric devices. In comparison to the photographic plate these detectors provide a better accuracy, better linearity and a wider dynamic range. However, they are essentially "single pixel" devices and can only deal with one object at a time.

Some photographic studies were made as well, chiefly of extended objects like galaxies, nebulae or star fields. An interesting stellar instrument was proposed and investigated by Treanor [1968]. He was looking for an effective way to determine the polarization angle of a large star field to trace the Galactic magnetic field. His approach will be briefly described in Chapter 2. A development of his concept is the theme of this Thesis.

Charge-Coupled Devices (CCDs) now available provide better quantum efficiency (about 10-100 times better than photography [Ratledge, 1997]) and better linearity. From the time when they became available, CCDs were soon applied to polarimetry [e.g. see Röser and Meisenheimer, 1986].

1.2 Development of a high accuracy CCD-Polarimeter

The development of new instruments for stellar polarimetry (wide colour-band) is still of interest — particularly if accuracy can be improved. This can be done by collecting and utilizing more photons, so improving the signal-to-noise ratio.

If bright objects are to be observed, the photon count rate has practical limitations. In the case of photomultipliers, the limitation is due to dead time problems. In modern polarimetric systems, the signals of the photomultiplier are recorded by photon counting techniques. If the photo-electron production rate is high, pulse overlap occurs and the signal becomes non-linear. For bright stars, neutral density filters are often used to reduce the photon rate — this defeating the purpose of using telescopes to collect the photons in the first place!

If CCDs are used, there is a similar problem. The total photon count is limited by the full-well capacity of each pixel and the number of pixels used.

One possibility of accepting the potentially large signals from bright stars is by spreading the light into many detectors — for example using many pixels of the CCD, each acting as a small 'light bucket'. Out of focus imaging explored by Clarke and Naghizadeh-Khouei [1997] provides such a technique with potential for high accuracy polarimetry.

Another possible technique to spread the light into many pixels of the CCD is based on the "ring-polarimeter" developed by Treanor [1968] as mentioned earlier. It uses a fast rotating tilted glass plate placed in the telescopes converging beam. This results in the light being spread over the area of a ring. With a polaroid attached to the rotating glass plate the polarimetric information of the light source is encoded on the circle and can be extracted.

The topic of this Thesis is to explore this concept of a "ring-polarimeter" in association with a CCD detector.

There are obvious differences as to how the data are reduced depending on whether photographic plates are employed or the record is made using CCDs. An important difference is the fact that plates provide detection-centers which are essentially distributed at random while the pixels of a CCD comprise a regular matrix. Thus, when it comes to analyzing data by assessing sections of the image, regular photographic plates will have the same sampling rate no matter the direction of the cut. In contrast the sampling rate with CCD-images will vary, with the sampling rate being highest along the axes of the pixel grid. Another important difference is that the CCD provides the data in digital format that can be directly processed by appropriate software, whereas the data of the photographic plate have to be gleaned by means of subsidiary laboratory machines such as micro-densitometers with their associated problems.

To investigate Treanor's method, adapted to modern technology, a prototype polarimeter has been built as described in Chapter 2. The theoretical description of the polarimeter is outlined in Chapter 3. To analyze the obtained data, specially developed software needed to be written. This is described in Chapter 4. The prototype was tested, both in the laboratory and at the observatory. In Chapter 5 it is shown how the test data have been reduced and analyzed and the results will be discussed. In Chapter 6 the experiences with the prototype will be discussed and proposals will be made for the next generation of CCD-Ring-Polarimeters.

2

The prototype CCD-Polarimeter

2.1 Treanor's "ring-polarimeter"

The general setup of the prototype CCD-Polarimeter is based on Treanor's [1968] "ring-polarimeter". The main feature of Treanor's device is a rotatable cell placed just in front of the photographic plate in the telescope's focal plane. The cell contains a polaroid placed in front of an inclined plane parallel glass plate (see Fig. 2.1). The

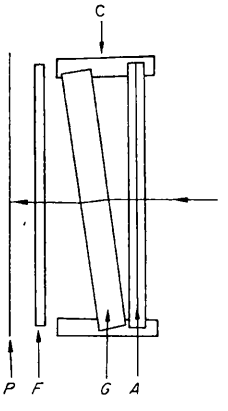

Fig. 2.1. Original diagram of Treanor's ring-polarimeter: P, photographic plate; F, filter; G, inclined plane parallel glass plate; A, analyzing polaroid; C, rotating cell.

glass plate serves merely to displace the star images, so that rotation of the cell will convert the point-like images into rings. For an unpolarized star, the ring will be uniform in intensity. For a completely polarized star, however, there are two orientations of the polaroid at which the star-light is completely extinguished. Therefore the intensity of the ring is strongly modulated around its circumference, so that it adopts the appearance of two French croissants, horn-to-horn (see Fig. 2.2).

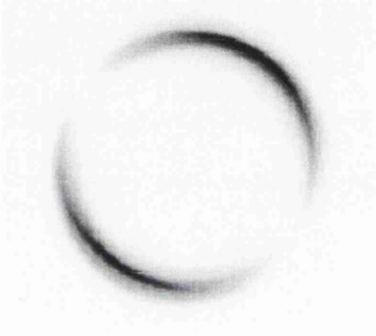

Fig. 2.2. Picture of an artificially polarized star, recorded with the CCD-Polarimeter.

2.2 Construction of the prototype CCD-Polarimeter

The CCD-Polarimeter has been built following the optical principals of Treanor's "ring-polarimeter". The main difference is the use of a modern CCD camera as photon counting device instead of the original photographic plate. Another difference is the use of a glass wedge to deviate the light beam instead of a tilted glass plate. The reason for this change was simply the better availability of glass wedges with optical quality.

The prototype instrument was essentially a bread-board model with most of the elements being scavenged from discarded equipment. Although in the end the modulator system might be applied to any telescope, it was decided to test out the polarimetric principles by making a stand alone instrument complete with its own small telescope.

By doing this, bright stars could be investigated, something that larger telescopes are just too big to allow.

A sketch of the setup is shown in Fig. 2.4. A telescope (**a**) with a focal length of 350mm and a diameter of 75mm is connected to a flip mirror (**b**). This flip mirror allows the light to be sent either to an ocular, for purposes of alignment, or through the aluminium box to the CCD. In the box the light beam passes through several optical elements. First there is a selection of different colour filters mounted on a wheel (**c**). This wheel is mechanically connected to a control outside the box so that it is possible to change the filters without opening the box.

Immediately following the filter wheel comes the analyzer (**d**). A rotatable cell that, in the final design, contains a polaroid (**e**) placed in front of an anti-reflective glass wedge (**f**). The glass wedge has one face inclined to the other by $\sim 1.5°$. It has a similar effect like the inclined plane parallel glass plate Treanor used. The beam is deviated by a small angle; when the cell is rotated, the point-like star images are transformed into ring images. Unpolarized stars will have a flat intensity distribution around the circumference, a polarized star instead will have a $\cos 2\alpha$ modulated intensity distribution. The form of the modulation for generally partially polarized light will be derived mathematically in Chapter 3.

Some other possibilities to analyze the beam of light have been tested: First a thick superachromatic half-waveplate was inserted in the rotatable tube at an angle so that the beam of light is deviated. In addition a fixed polaroid was placed just in front of the CCD camera at (**i**). With this design the ring image of a polarized star will have a $\cos 4\alpha$ modulated intensity distribution along its circumference (see Fig. 5.2 on page 40). Thereafter, an analyzer similar to the final version has been tried, but with a tilted glass plate in the form of a beam splitter instead of the glass wedge. In Chapter 5 the experiences with the different methods will be presented.

The analyzer is embedded in a ball-race and connected with several gear wheels to an electric, synchronised AC motor (**g**) that is attached at the outside of the box. The motor, produced by FRACMO LTD. London, performs 500 revolutions per minute. During exposure the motor will be running, and the cell is rotated by $\sim$ 715 rev/min with a gear transmission ratio of 1.43.

Behind the analyzer, a 50 mm photographic lens (**h**) is mounted on an optical bench. Its purpose is to reimage the focus further out and this way providing more space for the different optical elements. By moving the 'transfer-lens' on the bench, the image can be focused onto the CCD chip. The last element in the box is an optional polaroid (**i**). Finally a CCD camera (**k**) is plugged in a socket at the outside of the box.

The box was mounted on a thick aluminium plate that could be screwed on to the Grubb-Parsons 20-inch (0.5m) telescope at the Cochno observatory, simply used as a platform for guiding purposes. Additional connecting bars and damping materials were used to reduce the effect of vibration to a minimum.

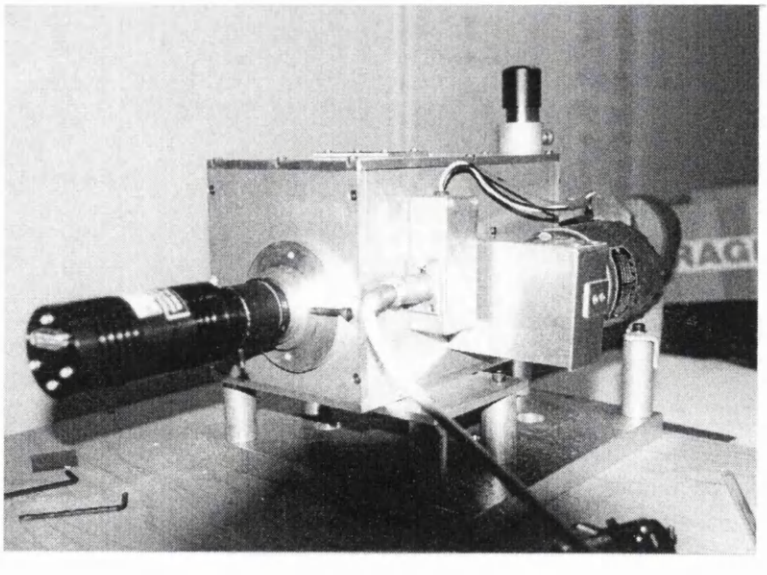

Fig. 2.3. Picture of the CCD-Polarimeter

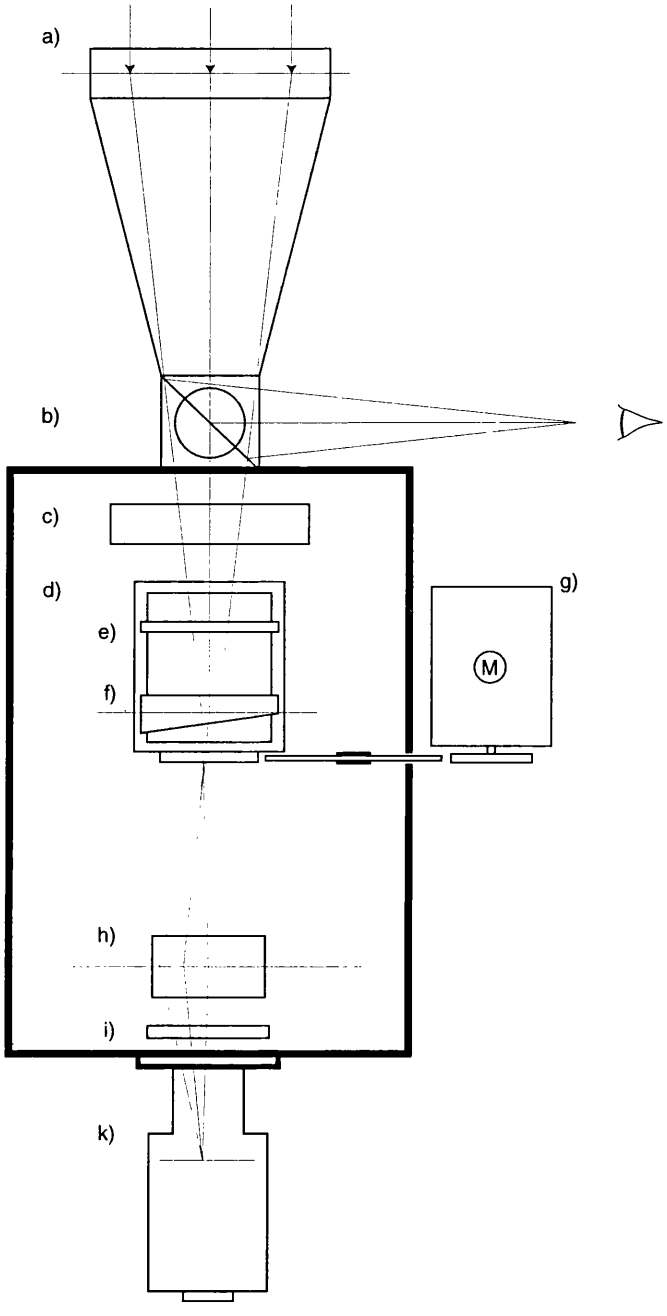

Fig. 2.4. The cross-sectional drawing of the setup of the prototype is shown: **a)** 75mm telescope; **b)** flip mirror; **c)** wheel containing a variety of different filters that can be positioned in the light beam; **d)** the analyzer: a metal tube, held in a ball-race, that contains **e)** a polaroid followed by **f)** a glass wedge; **g)** AC motor that drives the rotatable cell; **h)** 50 mm lens; **i)** optional polaroid; **k)** CCD camera. Overlaid on the diagram, a sketch of three light paths is shown to emphasize the purpose of the glass wedge (the beam is deviated) and the 'transfer-lens' (focus is reimaged).

2.2.1 The advantages of the design

The design outlined above has several advantages:

- Changes in sky transparency are averaged out over the measurement.
- One frame or one exposure contains all necessary information to determine the normalized Stokes parameters and the polarization angle.
- By choosing a suitable wedge according to its angle either a large star field can be analyzed at once (see Fig. 4.4 on page 31) or alternatively one bright star can be analyzed with high accuracy.

2.2.2 Details of the CCD camera

As photon recording device a CCD camera HX516 from Starlight-Xpress was used. It provides an actively cooled CCD chip with 660×494 pixels and a 16 bit interface. The HX516 comes with a Windows based control and processing program, PIX_H5. Although this software package has its bugs (see Section 4.1 on page 24) the overall performance has been satisfactory.
The HX516 camera specification:

- **CCD type**: Sony ICX084AL HyperHAD CCD with ultra low dark current and vertical anti-blooming.
- **CCD pixel data**: Pixel size: 7.4 x 7.4μm, Image format: 660 x 494 pixels (unbinned). In 2 x 2 binned mode - Pixel size: 14.8 x 14.8μm, Image format: 330 x 247 pixels.
- **CCD size**: Imaging area: 4.9mm (horizontal) x 3.6mm (vertical).
- **Spectral response**: Peak response at 520nm (green), 50% at 400nm (violet) and 670nm (near infra-red).

- **Readout noise**: Approx. 15 electrons RMS.
- **Full-well capacity**: Approx. 40,000 e^- (160,000 binned).
- **ADC factor**: 0.75 e^-/ADU unbinned, 1.5 e^-/ADU binned [Platt, 2000].
- **Anti-blooming**: Overload margin greater than 800x.
- **Dark current**: Typical dark frame saturation time longer than 150 hours. Less than 0.1 electrons/pixel/second.
- **Data format**: Full 16 bits.
- **Computer interface**: 8 bit unidirectional parallel port with bi-directional status lines (Standard Centronics interface). 25 pin 'D' style plug for LPT1, 2 or 3, via a 5 metre x 6mm diameter cable.
- **Cooling system**: Regulated constant-current cooling supply built-in. Single-stage thermoelectric cooler to give a CCD temperature of approximately $-30°C$ below ambient.
- **Size**: 50 x 100mm black anodised aluminium barrel with M42 thread at CCD window end and 15 way 'D' style input plug at rear.
- **Weight**: 200g.

2.3 Instrumental effects in CCD detectors

To get clean data with a CCD, a few of its imaging characteristics need to be taken into account. The raw images returned by a CCD contain a number of instrumental effects which must be removed before the image can be used for quantitative purposes.

Bias and Thermal Noise

Usually the amplifier which boosts the signal prior to its digitisation by the analogue-to-digital converter will also generate an offset (bias), which is added to the real signal generated by illuminating photons. A technique to estimate the bias is to take several short exposures with closed shutter and then average the frames. The resulting 'master' bias frame is then simply subtracted from the image frames.

Another effect which is sometimes present is an offset from zero that is generated thermally within the CCD chip, even when no light is present. It varies somewhat from pixel to pixel and can be minimized by cooling the CCD. It can be measured by taking long exposures with the shutter closed, removing the bias and dividing by the exposure time. This dark frame can then be scaled to the exposure time of the image frame and subtracted from the latter.

A very convenient way to correct image frames for both effects, the bias and the thermal noise, is to simply obtain exposures with exactly the same exposure time as the actual image frames, but with closed shutter. Averaging these dark frames and then subtracting them of the image frames gives the necessary corrections.

Variation in Pixel sensitivity, flat fielding

The sensitivity of the pixels will vary slightly across the CCD grid, due to imperfections in the manufacturing process. The relative sensitivities of the pixels can be calibrated by acquiring several images of an evenly illuminated source, such as the twilight sky or the inside of the dome. Having these so called flat fields allows calculation of a master flat field (MFF) that is normalized to a mean intensity of unity. By dividing image frames by this MFF, the images are calibrated. The flat fielding procedure also corrects for inequalities introduced by filters and other optical elements. Therefore it is important, that the flat fields are taken at the same conditions like the real frames, e.g. with the same filters and with rotating analyzer in the case of the prototype CCD-Polarimeter.

3

Theory of the polarimeter

3.1 Mathematical description of the polarimeter

As shown in Chapter 2, the main part of the CCD-Polarimeter consists of a rotating tube that contains either a half-waveplate or a polarizer. These arrangements can be expressed in mathematical terms using Stokes parameters and Mueller calculus (see Appendix A). Optical elements such as a polaroid or a half-waveplate can be expressed by matrices (see table A.1) and a beam of light can be described by a Stokes vector (e.g. $S = [I, Q, U, V]^{\mathsf{T}}$).

3.1.1 Rotating Polarizer

Since the axes of the polaroid are rotated at an angle α to the reference frame of the initial signal S, which is the reference frame of the fixed CCD camera, the Stokes vector of S has to be converted to the axes of the polaroid by multiplying the vector with the rotation matrix $[\mathsf{R}(\alpha)]$. Then the beam of light passes through the polaroid, represented by the polarization matrix $[\mathsf{P}]$. Now it has to be rotated back to the reference frame

of the CCD by multiplying the vector with the rotation matrix $[\mathsf{R}(-\alpha)]$. In short we have:

$$S^* = [\mathsf{R}(-\alpha)] \cdot [\mathsf{P}] \cdot [\mathsf{R}(\alpha)] \cdot S \quad . \tag{3.1}$$

Using matrix notation, the received signal can be calculated:

$$\begin{bmatrix} I^* \\ Q^* \\ U^* \\ V^* \end{bmatrix} = [\mathsf{R}(-\alpha)] \frac{1}{2} \begin{bmatrix} 1 & 1 & 0 & 0 \\ 1 & 1 & 0 & 0 \\ 0 & 0 & 0 & 0 \\ 0 & 0 & 0 & 0 \end{bmatrix} \begin{bmatrix} 1 & 0 & 0 & 0 \\ 0 & \cos(2\alpha) & \sin(2\alpha) & 0 \\ 0 & -\sin(2\alpha) & \cos(2\alpha) & 0 \\ 0 & 0 & 0 & 1 \end{bmatrix} \begin{bmatrix} I \\ Q \\ U \\ V \end{bmatrix} \tag{3.2}$$

$$\begin{bmatrix} I^* \\ Q^* \\ U^* \\ V^* \end{bmatrix} = [\mathsf{R}(-\alpha)] \frac{1}{2} \begin{bmatrix} 1 & 1 & 0 & 0 \\ 1 & 1 & 0 & 0 \\ 0 & 0 & 0 & 0 \\ 0 & 0 & 0 & 0 \end{bmatrix} \begin{bmatrix} I \\ Q\cos(2\alpha) + U\sin(2\alpha) \\ -Q\sin(2\alpha) + U\cos(2\alpha) \\ V \end{bmatrix} \tag{3.3}$$

$$\begin{bmatrix} I^* \\ Q^* \\ U^* \\ V^* \end{bmatrix} = \begin{bmatrix} 1 & 0 & 0 & 0 \\ 0 & \cos(-2\alpha) & \sin(-2\alpha) & 0 \\ 0 & -\sin(-2\alpha) & \cos(-2\alpha) & 0 \\ 0 & 0 & 0 & 1 \end{bmatrix} \frac{1}{2} \begin{bmatrix} I + Q\cos(2\alpha) + U\sin(2\alpha) \\ I + Q\cos(2\alpha) + U\sin(2\alpha) \\ 0 \\ 0 \end{bmatrix} \tag{3.4}$$

Since the CCD is only[1] sensitive to the intensity of light, the observed quantity is $I^*(\alpha)$ whereas Q^*, U^* and V^* are not taken into account. The formula for the received signal $I^*(\alpha)$ is then:

$$I^*(\alpha) \quad = \quad \frac{1}{2}\big(I + Q\cos(2\alpha) + U\sin(2\alpha)\big) \tag{3.5}$$

[1]For the purposes of the development here, it is assumed that CCD detectors are insensitive to any polarization in their illumination, and respond only to the total flux received.

It can be seen that the received signal comprises a constant level ($\frac{1}{2}I$) with a superimposed modulated component with frequency twice that of the rotating polaroid (analyzer).

Only I, Q and U of the original Stokes vector contribute to the received intensity, the V part is filtered out in this method of measurement.

Getting the Stokes parameters q and u

Three different equations are needed to get the three unknown variables I, Q and U. One approach involves integrating $I^*(\alpha)$ over three different ranges of α. Assuming the polarizer rotates N times during exposure, so producing N overlaid circles, the equations are:

$$S_1 = N\int_0^{2\pi} I^*(\alpha)\, d\alpha = N\pi I \tag{3.6}$$

$$S_2 = N\int_0^{\frac{\pi}{2}} I^*(\alpha)\, d\alpha + N\int_{\pi}^{\frac{3\pi}{2}} I^*(\alpha)\, d\alpha = \quad 2N\int_0^{\frac{\pi}{2}} I^*(\alpha)\, d\alpha = N\left(\frac{\pi}{2}I + U\right) \tag{3.7}$$

$$S_3 = N\int_{\frac{\pi}{4}}^{\frac{3\pi}{4}} I^*(\alpha)\, d\alpha + N\int_{\frac{5\pi}{4}}^{\frac{7\pi}{4}} I^*(\alpha)\, d\alpha = \quad 2N\int_{\frac{\pi}{4}}^{\frac{3\pi}{4}} I^*(\alpha)\, d\alpha = N\left(\frac{\pi}{2}I - Q\right) \tag{3.8}$$

The normalized Stokes parameters q and u may then be derived as

$$q = \frac{Q}{I} = \pi\left(\frac{1}{2} - \frac{S_3}{S_1}\right) \tag{3.9}$$

$$u = \frac{U}{I} = \pi\left(\frac{S_2}{S_1} - \frac{1}{2}\right) \tag{3.10}$$

The degree of polarization is calculated by

$$p = \sqrt{q^2 + u^2} \tag{3.11}$$

One of the benefits of this formalism is that it concentrates on the $2 + 4n$ harmonics, $n = 0, 1, 2, 3...$ — all other harmonics do not contribute to the integration.

In the case of the CCD-Polarimeter, the signals $S_{1,2,3}$ are measured in arbitrary units of so-called 'analogue data units' (ADU). Usually they have to be multiplied with the ADC factor G which is the constant of proportionality to convert ADUs into the amount of charge (expressed as number of photon-electrons) stored in the pixels. For the calculation of the normalized Stokes parameters this factor is not needed because it cancels out. For the calculations of the influence of measurement uncertainties, G must be taken into account, however.

Computation of errors

Estimates for the errors associated with the measurements are based on photon counting statistics. Since the values of q and u are obtained at least partially over the same parts of the modulation profile, effects of noise introduce a correlation between the determined normalized Stokes parameter. As Stewart [1985] shows in his Research Note, this results in an increased uncertainty region for the true values (q_0, u_0) on the $q - u$ plane. He shows also that *"under situations where polarizations are* $< 10\%$ *and ... if the photon count per measurement is greater than a few thousand, the correlation effects are insignificant."* In our case we have a high photon count (usually $\sim 4 \times 10^5$) which allows us to neglect this correlation and to assume that σ of each pixel value $G \times v$ is $\sqrt{G \times v}$, with G being the ADU conversion factor. To calculate the errors, Gaussian error propagation is used which in general form is

$$\Delta f(x,y) = \sqrt{\left(\frac{\delta f}{\delta x}\Delta x\right)^2 + \left(\frac{\delta f}{\delta y}\Delta y\right)^2} \tag{3.12}$$

For the normalized Stokes parameters the errors are as follows:

$$\Delta q = \frac{1}{\sqrt{G}}\sqrt{\left(\frac{-\pi}{S_1}\sqrt{S_3}\right)^2 + \left(\frac{\pi S_3}{(S_1)^2}\sqrt{S_1}\right)^2} \tag{3.13}$$

$$\Delta u = \frac{1}{\sqrt{G}}\sqrt{\left(\frac{\pi}{S_1}\sqrt{S_2}\right)^2 + \left(\frac{-\pi S_2}{(S_1)^2}\sqrt{S_1}\right)^2} \tag{3.14}$$

$$\Delta p = \frac{1}{\sqrt{G}}\sqrt{\frac{q^2(\Delta q)^2 + u^2(\Delta u)^2}{q^2 + u^2}} \tag{3.15}$$

In the special case of an unpolarized star we have:

$$S_2 = S_3 = \frac{S_1}{2} \quad \rightarrow \quad \Delta p = \frac{\pi}{\sqrt{G}}\sqrt{\frac{3}{4S_1}} = \sqrt{\frac{3\pi}{4GNI}} \tag{3.16}$$

To increase the accuracy of the polarimeter, a high photon count (GNI) is important. Since the capacity of each pixel is limited, it is useful to spread the light over a larger area of pixels. For example the ring image of an out of focus star with outer radius $r_{out} = 100$ pixels, inner radius $r_{in} = 80$ pixels uses about 22500 pixels. If e.g. 20000 photons may be counted by each pixel the total photon count is 4.5×10^8 and the accuracy of p is about $\pm 7 \times 10^{-5}$.

3.1.2 Rotating half-waveplate version

For completeness the derivation of the intensity modulation for the rotating half-waveplate version will be shown. It was only used for first tests of the polarimeter in the laboratory and was not run using real stars. Consequently the computation of errors and the determination of the normalized Stokes parameters will not be presented. Generally this kind of modulation has the advantage that the detector receives a constant direction of vibration of polarized light. For this design the polarimeter consists of a rotating HWP, followed by a fixed polaroid. Since the axes of the HWP are rotated at an angle α to the reference frame of the CCD camera and the fixed polaroid, the Stokes vector of the incoming signal S, which is referred to the reference frame of the CCD camera, has to be converted into the reference frame of the rotating HWP,

by applying a rotation matrix $[\mathsf{R}(\alpha)]$. Then the beam passes the HWP, represented by $[\Delta = \pi]$. Now it has to be rotated back $[\mathsf{R}(-\alpha)]$ and pass through the polaroid $[\mathsf{P}]$.

In short:

$$S^* = [\mathsf{P}]\,[\mathsf{R}(-\alpha)]\,[\Delta = \pi]\,[\mathsf{R}(\alpha)] \cdot S \tag{3.17}$$

The matrix calculation, using a general retarder $[\Delta]$ is developed as follows:

$$\begin{bmatrix} I^* \\ Q^* \\ U^* \\ V^* \end{bmatrix} = [\mathsf{P}]\,[\mathsf{R}(-\alpha)]\,[\Delta] \begin{bmatrix} 1 & 0 & 0 & 0 \\ 0 & \cos(2\alpha) & \sin(2\alpha) & 0 \\ 0 & -\sin(2\alpha) & \cos(2\alpha) & 0 \\ 0 & 0 & 0 & 1 \end{bmatrix} \begin{bmatrix} I \\ Q \\ U \\ V \end{bmatrix}$$

$$\begin{bmatrix} I^* \\ Q^* \\ U^* \\ V^* \end{bmatrix} = [\mathsf{P}]\,[\mathsf{R}(-\alpha)] \begin{bmatrix} 1 & 0 & 0 & 0 \\ 0 & 1 & 0 & 0 \\ 0 & 0 & \cos\Delta & \sin\Delta \\ 0 & 0 & -\sin\Delta & \cos\Delta \end{bmatrix} \begin{bmatrix} I \\ Q\cos(2\alpha) + U\sin(2\alpha) \\ -Q\sin(2\alpha) + U\cos(2\alpha) \\ V \end{bmatrix}$$

$$\begin{bmatrix} I^* \\ Q^* \\ U^* \\ V^* \end{bmatrix} = [\mathsf{P}] \begin{bmatrix} 1 & 0 & 0 & 0 \\ 0 & \cos(-2\alpha) & \sin(-2\alpha) & 0 \\ 0 & -\sin(-2\alpha) & \cos(-2\alpha) & 0 \\ 0 & 0 & 0 & 1 \end{bmatrix} \begin{bmatrix} I \\ Q\cos(2\alpha) + U\sin(2\alpha) \\ \cos\Delta(-Q\sin(2\alpha) + U\cos(2\alpha) + V\sin\Delta \\ -\sin\Delta(-Q\sin(2\alpha) + U\cos(2\alpha) + V\cos\Delta \end{bmatrix}$$

Assuming no circular polarization ($V = 0$):

$$\begin{bmatrix} I^* \\ Q^* \\ U^* \\ V^* \end{bmatrix} = \frac{1}{2} \begin{bmatrix} 1 & 1 & 0 & 0 \\ 1 & 1 & 0 & 0 \\ 0 & 0 & 0 & 0 \\ 0 & 0 & 0 & 0 \end{bmatrix} \begin{bmatrix} I \\ Q\big(\cos^2(2\alpha) + \cos\Delta\sin^2(2\alpha)\big) + U\cos(2\alpha)\sin(2\alpha)(1-\cos\Delta) \\ \cdots\cdots\cdots\cdots\cdots\cdots\cdots\cdots\cdots\cdots\cdots\cdots \\ \cdots\cdots\cdots\cdots\cdots\cdots\cdots\cdots\cdots\cdots\cdots\cdots \end{bmatrix}$$

Again, since the CCD is only sensitive to the intensity of light, the observed quantity is $I^*(\alpha)$. The modulation of the received signal $I^*(\alpha)$ is then:

$$I^*(\alpha) = \frac{1}{2}\Big(I + Q\big(\cos^2(2\alpha) + \cos\Delta\sin^2(2\alpha)\big) + U\cos(2\alpha)\sin(2\alpha)(1-\cos\Delta)\Big)$$

Using the relation $\cos^2\alpha - \sin^2\alpha = \cos(2\alpha)$:

$$I^*(\alpha) = \frac{1}{2}\Big(I + Q\big(\cos(4\alpha) + \sin^2(2\alpha)\big[1+\cos\Delta\big]\big) + \frac{U}{2}\big(\sin(4\alpha)(1-\cos\Delta)\big)\Big) \tag{3.18}$$

With $\Delta = \pi$ for a half-waveplate, the wave form reduces to the form:

$$I^*(\alpha) \quad = \quad \frac{1}{2}\big(I + Q\cos(4\alpha) + U\sin(4\alpha)\big) \tag{3.19}$$

Thus, for this arrangement, the received signal consists of a constant level ($\frac{1}{2}I$) with a superimposed modulated component with frequency four times the frequency of the rotating half-waveplate.

In this chapter a formalism was derived to calculate the normalized Stokes parameters. In order to apply these formulas to the CCD data, a specialized software program was developed. The main procedures of this software will be described in the following chapter.

4

Software

Due to the uniqueness of the obtained images, specially developed software was required to reduce and analyze the data. This software should be able to

1) identify the circles and determine their centres and radii

2) produce an intensity profile along the circumference of each circle

3) determine the degree of polarization

Initially, the programming was done in a `UNIX` environment. The `GNU C++` compiler `gcc` was used to compile the code. Later, to allow the software to be used directly at the observatory, the code has been ported to `WIN32`, using the freely available `cygwin` package.

Before starting to explain the actual analyzing program, another problem needs to be mentioned. During the work on this project it was noticed that the software package provided by the camera (PIX_H5 V2.2 b) does not produce standard output files. An extra program had to be written to do the necessary conversions. In the following section this program (`FITCONV`) will be explained. The analyzing program (`ANALYSE`) will be described in Section 4.2.

4.1 FITCONV explained

4.1.1 The problem with PIX_H5

First of all, it is important to know how the raw data files are formatted. In our case the image files are stored in the Flexible Image Transport System format (FITS). These files contain FITS-Keywords such as EXPTIME (exposure time) or OBJECT and a two dimensional image array corresponding to 600x550 pixels. Each pixel is stored as a 16 bit value, resulting in an integer range of 0-65535.

Unfortunately it turned out that the PIX_H5 software does not comply to the FITS standard in the way it stores these pixel values. The problem is that PIX_H5 saves the values as unsigned integers although FITS doesn't directly support unsigned integers. The convention used in FITS files is to store the unsigned integer data values as signed integers with an associated offset (specified by the BZERO keyword). For example, to store unsigned 16-bit integer values in a FITS image, the image should be defined as a signed 16-bit integer with the keyword BZERO = 32768. Thus the unsigned values of 0, 32768 and 65535 for example, are physically stored in the FITS image as -32768, 0, and 32767, respectively.

4.1.2 Correcting the files

The program works fairly simply thanks to the CFITSIO package provided by HEASARC [Pence, 1999]. It provides many useful and easy to use routines for handling FITS files. First the image is read into an array. Then all values < 0 are corrected by adding 2^{16}.

For example the value 32772 would be stored by PIX_H5 as unsigned integer which is in dual notation 1000 0000 0000 0100 ($32772 = 2^{15}+2^2$). However, any other software that conforms to the FITS standard will interpret this value as signed integer and return -32764 ($-32764 = -2^{15} + 2^2$). Adding 2×2^{15} therefore restores the original value.

Then the corrected data array is saved as FITS again using a `CFITSIO` routine. This routine follows the above mentioned convention and stores the values according to the FITS specification as signed integers with an associated offset. Care was taken to make sure that the original keywords, if not already set by the save routine (like BZERO), are transferred to the new file. Empty `COMMENT` and `HISTORY` keywords are stripped off. Finally a new keyword `FITCONV` is appended to mark the file as converted.

As an example of the problem discussed above, Figure 4.1 on the next page shows an unconverted image and a slice taken at row 300 through the circle. It is obvious what has gone wrong. The range is -32768 to 32767 and the part of the image that should be brightest turns into dark colours (or to negative values). Figure 4.2 shows the converted image. Now the image is ready for further processing and analyzing.

a)

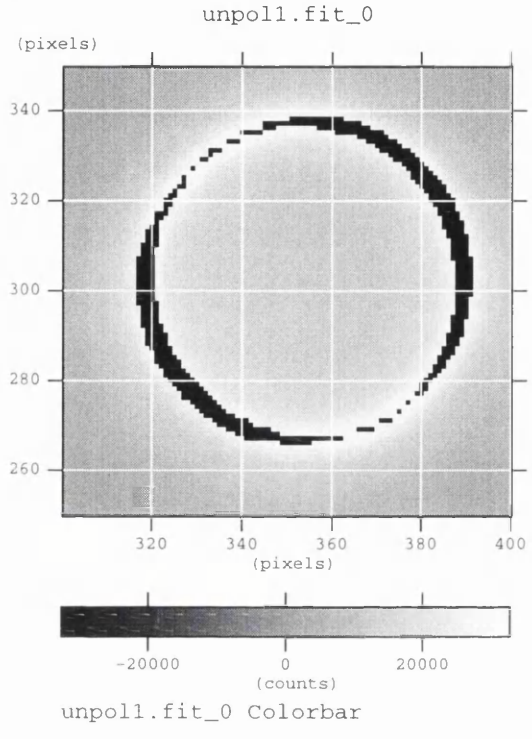

b)

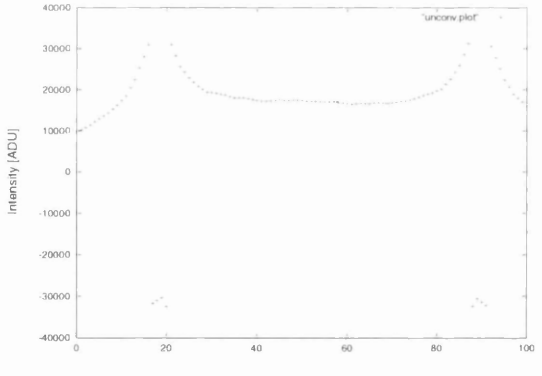

Fig. 4.1. a) Raw image with negative intensity values (shown as black colour).**b)** Intensity distribution along a slice cut in the middle of the circle (at row 300) showing intensity values dropping to negative values when reaching 32768.

a)

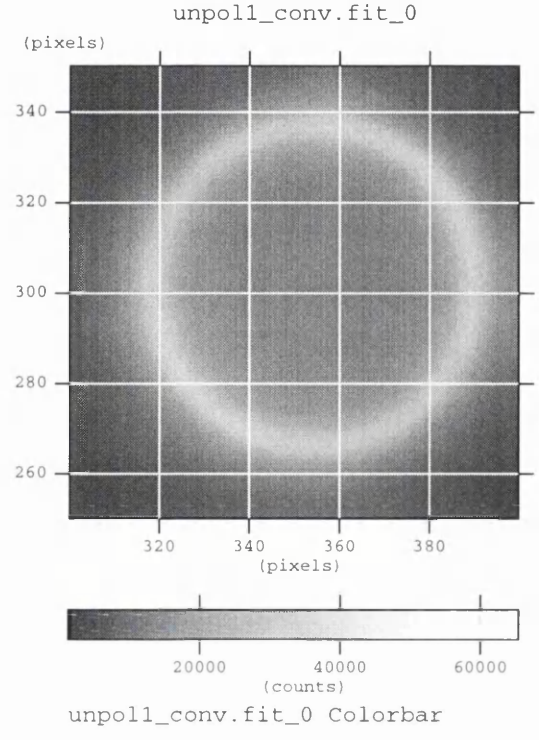

b)

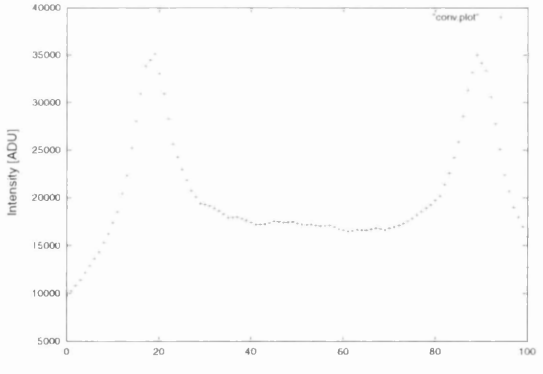

Fig. 4.2. a) Same image after converting with `FITCONV`, this time having a correct intensity range.**b)** Intensity distribution of row 300, showing a smooth curve and no negative intensity values after conversion.

4.2 ANALYSE explained

The `ANALYSE` program is divided into two parts. The first part (`main menu`) serves to find the circles. Therefore several commands are available. The positions and radii of the circular star images can either be typed in from the keyboard or automatically found using an algorithm that will be described in Section 4.2.2 in more detail. To facilitate the manual search for the circles, it is possible to plot intensity distributions along rows and columns. This function has been used to create Fig. 4.1 b) and Fig. 4.2 b) on page 26, for example.

The second part (`analyze menu`) serves to analyze the found circles. Here the degree of polarization of a selected circle can be computed and an intensity profile along the circumference can be plotted.

In the following sections some procedures and algorithms will be explained in more detail.

4.2.1 Accessing the data

The first task for the program is to access the data held in the CCD frames. As seen in Section 4.1, the input files are stored as FITS and contain a two dimensional image array of 500x660 16 bit integer values.

Since the data are in FITS format, it is not straight forward to actually transfer the data to the memory of the computer. The first approach was to use Starlink software to convert the FITS-files into ASCII-files, which then can be easily accessed by a simple C-routine. The scheme worked well but there were a few disadvantages:

1) The required disk-space for each file was easily tripled.

2) The conversion process was time consuming.

It would be neat and more "professional" to access the FITS files directly. An alternative package `CFITSIO` was available through Starlink but at the time was not installed in Glasgow. This was rectified and became the standard means to access and handle files in FITS format.

In the `load` routine (see Appendix B) `CFITSIO` routines are used to load the image data into a 500x660 integer array. Now it is time to find the circles.

4.2.2 Finding the circles

The general procedure to locate the circular images is to scan the data array row by row and search for peak intensities[1]. If more than one peak is found in a row r, their centres (row centres) are calculated $(cr_1...cr_n)$. Then, for all row centres $cr_1...cr_n$, the column that goes through the centre cr_i is scanned for peaks and their centres (column centers) are calculated $(cc_1...cc_n)$. Now, if a column centre cc_j lies on row r we have probably found the centre of a circle. To check on this, the distances of this point to the neighbouring peaks in the row and column are compared. If they match, this distance corresponds to the radius for the circle with centre at (cr_i, cc_j).

The algorithm described above was implemented using three functions. `rowscan(row)` scans a row for peaks and returns a table with the positions of the centres and the distances between the centre and their neighbouring peaks. `colscan(col)` works likewise with columns. These two functions are invoked by the function `scan` that at the end returns a table containing the circle centers and their radii.

The scan routine is controlled by two parameters: **d** and **base**. Both can be changed in the `main` menu.

1) **base** is a value that is multiplied with the average (mean intensity) of all pixels. Only pixels with higher values than $(base \times average)$ are candidates for peaks.

[1] A pixel is considered to be a peak intensity if **d** pixels on the right and left (or up and down) have lower intensity values. Parameter **d** can be changed in the main menu during runtime.

2) **d** determines how many pixels on the left and right (or up and down) of the regarded pixel have to have lower intensity values than the one itself to declare it a peak.

The flowchart (Fig. 4.3 on the following page) illustrates the scanning algorithm. On page 31 a prepared example (Fig. 4.4) shows a snapshot of the scanning process. The examined frame features a part of the Pleiades. This picture has been taken at an early stage of evolution of the CCD-Polarimeter using an inclined glass plate to deviate the light. The star images appear as ellipses due to problems with vibration. To illustrate how the circles are detected, intensity profiles along a row and a column are shown, both going through the center of a circle.

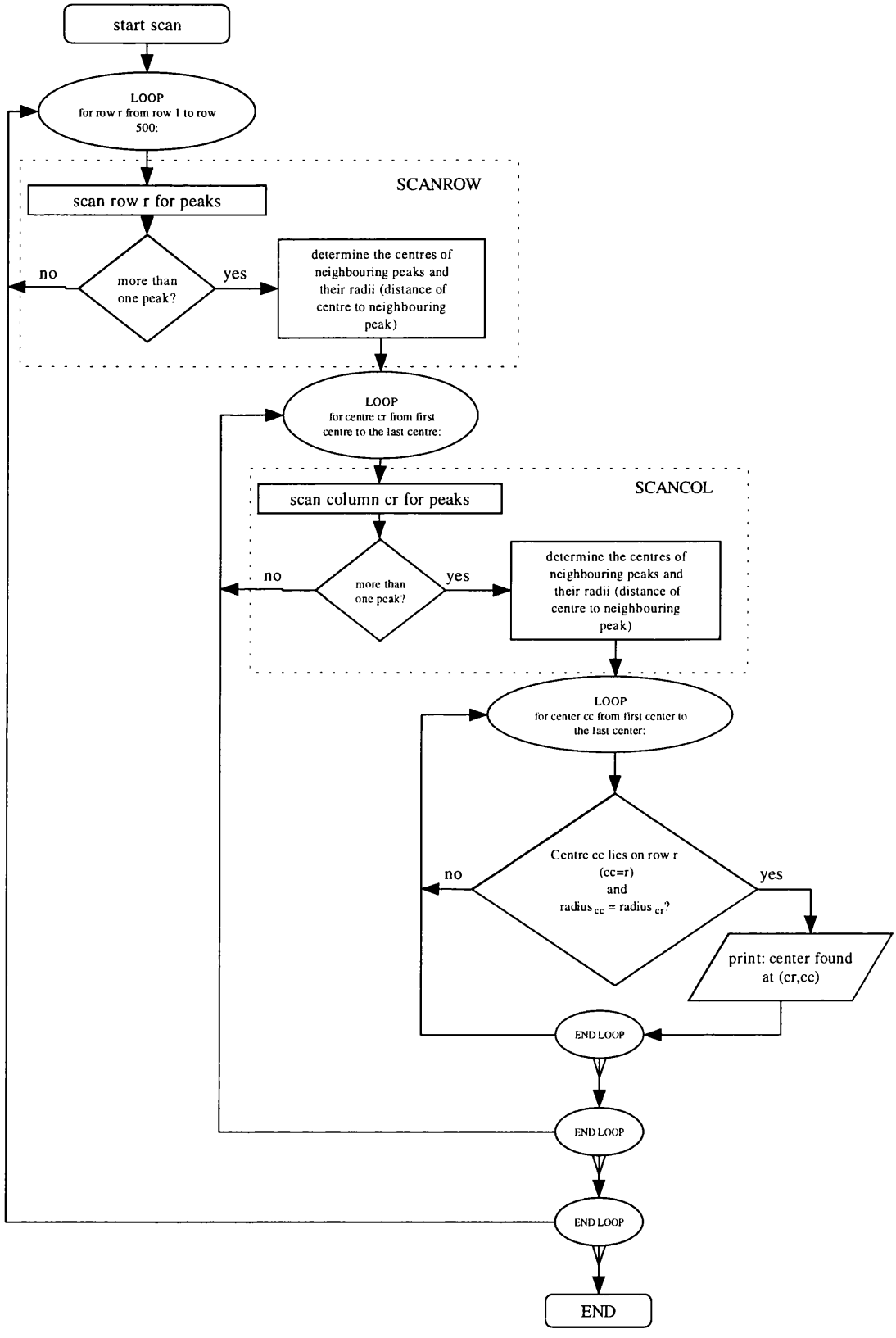

Fig. 4.3. Flowchart showing how the data array is scanned for circles

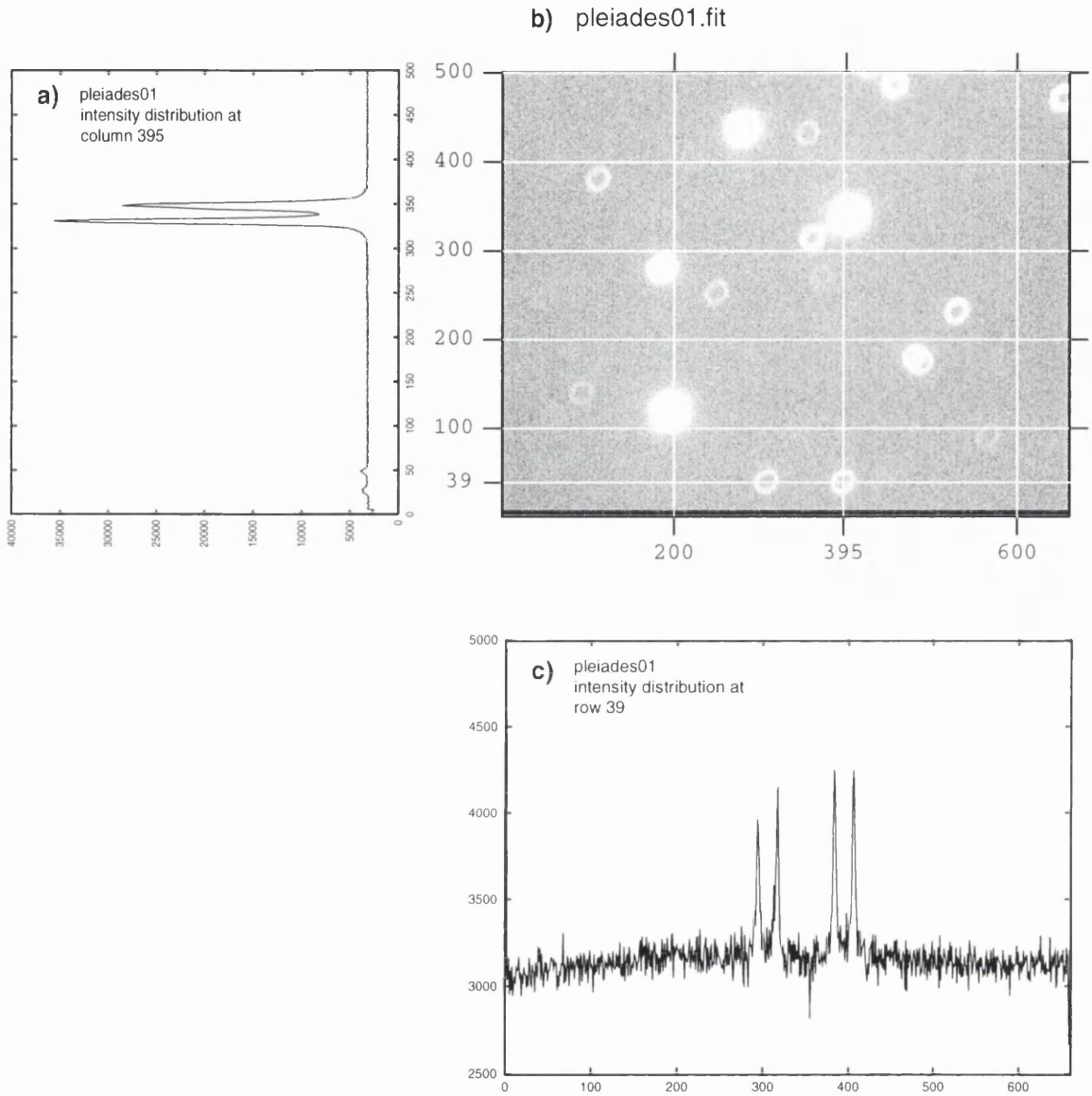

Fig. 4.4. A snapshot of the scanning process is shown. The examined frame, a part of the Pleiades, is displayed in **b)**. This picture has been taken at an early stage of evolution of the CCD Polarimeter. The star images appear as ellipses due to problems with vibration. Row 39 has just been scanned for peak intensities. Its intensity distribution is shown in **c)**. Four peaks have been found. For every center of two neighbouring peaks the according column is scanned. In **a)** the intensity distribution of column 395 is shown. This column corresponds to the center of the two peaks on the right. In column 395 peak intensities around 39, 190 and 341 are found. Since one of them matches with the position of the row (39) it is likely that a circle with center (395,39) has been found.

In the program, as soon as the table containing the circle properties is not empty, the `analyze` menu becomes available. Here, for a chosen circle, the intensity distribution along the perimeter can be plotted as a 2-D graph and the normalized Stokes parameters can be computed.

4.2.3 Determining the Stokes parameters

The normalized Stokes parameters q and u are calculated using the formulas (3.9) and (3.10), derived in Chapter 3:

$$q = \frac{Q}{I} = \pi\left(\frac{1}{2} - \frac{S_3}{S_1}\right); \quad u = \frac{U}{I} = \pi\left(\frac{S_2}{S_1} - \frac{1}{2}\right)$$

The values for S_1, S_2 and S_3 are obtained as follows: A ring around the center of the chosen circle with radius r is considered. The inner radius of the ring is $r_{in} = r - \textbf{range}$ and the outer radius is $r_{out} = r + \textbf{range}$.

The value for **range** is automatically determined as follows: First the position (r_{max}, α) on the circumference, where the intensity is maximum (I_{max}) is found. Then, starting from the center going towards (r_{max}, α) in radial direction the intensity profile is looked at. It is expected that the values will rise from background level to I_{max} and then fall back again. The two positions r_1 and r_2 where the intensity profile crosses the value $0.1 \times I_{max}$ are determined. This chosen value is arbitrary, but provides a realistic way of utilizing the majority of collected photons without introducing the noise from pixels containing responses to low light levels. The average of $|r - r_1|$ and $|r - r_2|$ gives the value for **range**. The range can be adjusted manually in the `analyze` menu.

Back to the ring. This ring is divided into 8 sectors of 45°, see Fig. 4.5.

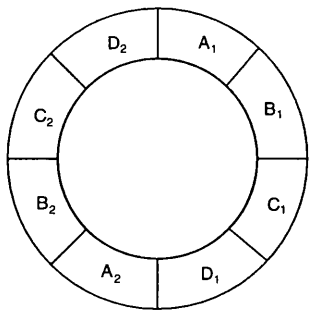

Fig. 4.5. Ring divided into 8 equally sized sectors.

The determination of S_1, S_2 and S_3 as shown in Chapter 3 corresponds to:

$$S_1 = A_1 + A_2 + B_1 + B_2 + C_1 + C_2 + D_1 + D_2 \tag{4.1}$$

$$S_2 = A_1 + A_2 + B_1 + B_2 \tag{4.2}$$

$$S_3 = B_1 + B_2 + C_1 + C_2 \tag{4.3}$$

Applying these integrations to Equations (3.9-11) allows q, u and p to be evaluated. To calculate the errors of q, u and p to their photon limit, the formulas derived in Chapter 3, 3.1.12-14 are used.

If the ring is not perfectly circular and the **range** is to small, a spurious $\sin(2\alpha)$ polarisation signal is produced. A similar effect is produced by an error in determination of the ring center, giving rise to a wrong modulation signal. These effects can be reduced by setting the **range** wide enough. The second effect is neglectable because the accuracy of determining the position of the centers is estimated to be ± 1 pixel. Compared to the size of the ring images of about 100 pixels in radius this is a small amount. Further, the pixels that might get lost because of a slightly displaced center are those at the border of the ring, containing only few more photons than the background.

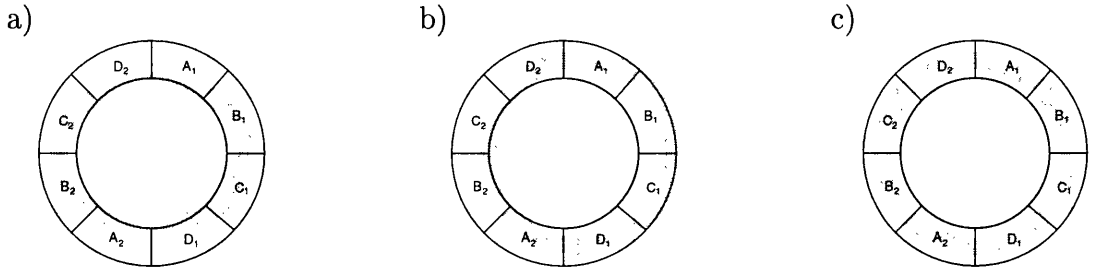

Fig. 4.6. These three illustrations show in an exaggerated manner how **a)** an elliptic ring may lead to a $\sin(2\alpha)$ signal or **b)** how a misplacement of the center will distort the signal. This happens because some pixels are outside of the range and the pixels in the sectors are not symmetrically distributed. The ideal case is shown in **c)**, a perfect circle correctly centered.

4.2.4 Plotting the intensity distribution along the perimeter of a selected circle

To demonstrate how the recorded intensity varies with the angle α, an intensity profile along the circumference can be plotted. This is achieved by scanning through pixels from the center of the circular image along various radius vectors with different angles α.

As the angular image is approached along such a radial scan, the recorded intensity will rise from the background level, achieve a maximum value near radius R and then fall away to the background. The position (R_{MAX}) of this maximum value is determined in the interval [$R\pm$ **flex**]. If the angular image were perfectly circular, the position R_{MAX} would match the radius R, but perhaps because of telescope tracking irregularities, this is almost never the case. Figure 4.7 on page 36 shows an intensity profile in a radial direction.

Now, the intensity values of the pixels in the interval [$R_{MAX}\pm$ **plotrange**] are summed up and stored in an array. The pixels which are interrogated are determined by stepping through this radial interval with a step-size of 1 pixel and converting the polar coordinates of these points (r, α) to their Cartesian positions (x, y). For values of $\alpha = 0°, 90°, 180°, 270°$ the converted coordinates match exactly the positions on the pixel grid. Since the CCD chip is an array of square pixels, for intermediate values

of α, the conversion provides a path along the radius which is not regular — the determined positions are floating point numbers and do not reflect points of the grid. By simply cutting off the decimal part they are converted to grid positions. More sophisticated interpolation schemes could be imagined. This simple method, however, produces smooth intensity profiles because the resolution of the CCD is very high and the image is spread somewhat in focus, giving a wider range.

This radial scanning is done for all angles α starting from 0° to 360° with steps of 1°. The sums of the intensity values are stored together with the according angle in an array. To actually show the graph of $I(\alpha)$, external software such as gnuplot can be used. Therefore the array is saved in an ASCII file. The parameter **bin**, that can be changed in the menu, determines the size of the bins. For example if **bin** is set as b, then $360/b$ bins are stored, containing the average value of b neighbouring values respectively.

The figures on the following page show the ring image of a star made polarized to 100% by placing a sheet polarizer prior to the telescope objective (Fig. 4.7). In Fig. 4.8 the radial intensity distribution for an arbitrary angle α is shown, together with the two intervals [$R\pm$ **flex**] and [$R_{MAX}\pm$ **plotrange**]. The final intensity profile along the circumference is displayed in Fig. 4.9, using a bin-size of 12°. It can be seen that the intensity varies with angle α according to $\cos(2\alpha)$ (Malus law, see page 3).

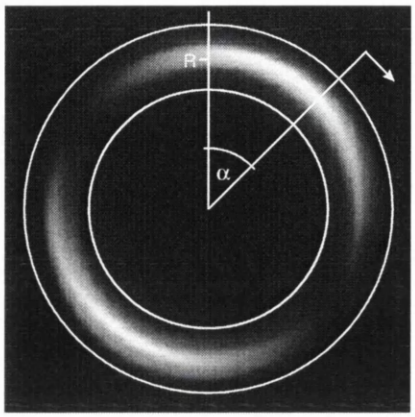

Fig. 4.7. It is shown how the circle is scanned azimuthally through all angles.

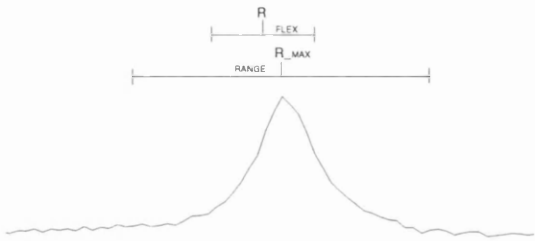

Fig. 4.8. Here a radial intensity distribution and the different ranges are shown. It can be seen that the position of R_{MAX} is not always identical with R.

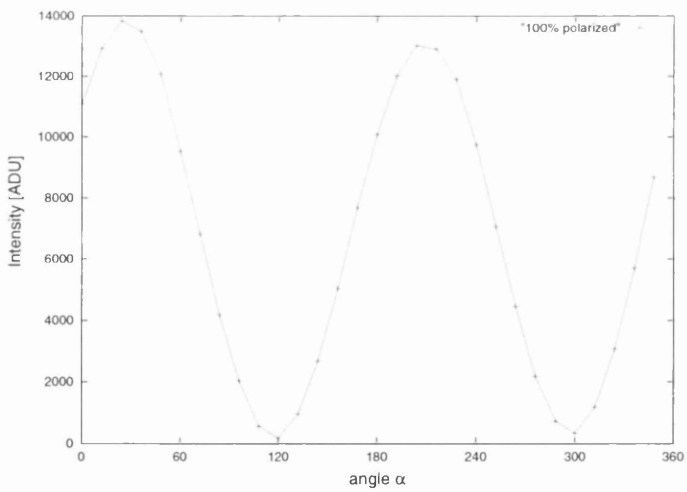

Fig. 4.9. The intensity profile along the circumference of Fig. 4.7, the ring image of a 100 % polarized star, is shown. The intensity varies with angle α according to $\cos(2\alpha)$ (Malus law).

5

The Polarimeter in practice

5.1 Tests in the Laboratory

In order to explore the feasibility of the polarimeter, trial experiments were set up in the laboratory. These allowed various optical modulators to be tested and provided sample frames to allow the development of the software as the polarimeter neared its more final form.

5.1.1 The setup of the experiment

The basement laboratory at the observatory in Acre Road, Glasgow was used, this being a long room, allowing an artificial star to be established at one end with the polarimeter attached to a bench at the other at a distance of approximately 10 metres. The 'star' is simply an ordinary light bulb behind a diaphragm, both mounted on a tripod, so that it could be aligned with the telescope. This arrangement guaranteed that experiments could be undertaken independent of the weather. There were, however, practical difficulties to overcome. The field of view of the telescope-CCD combination is small and it was difficult to 'find' the star. The motor vibration also caused a large

amount of image bounce. The polarimeter had to be fixed onto the bench with several clamps and additional heavy weights had to be placed on top of it to reduce the effect of vibration. Figure 5.1 shows a picture of the apparatus in the laboratory, with the weights on top of it.

The instrument had also been designed to use real stars at infinity, and adjustments were required to focus the laboratory artificial 'star'. To adjust the focus, the position of the transfer lens inside the box had to be set. Although mounted on an optical bench within the instrument, precise adjustment was very difficult. In retrospect, use of a gear rack instead of the optical bench would be a convenient remedy.

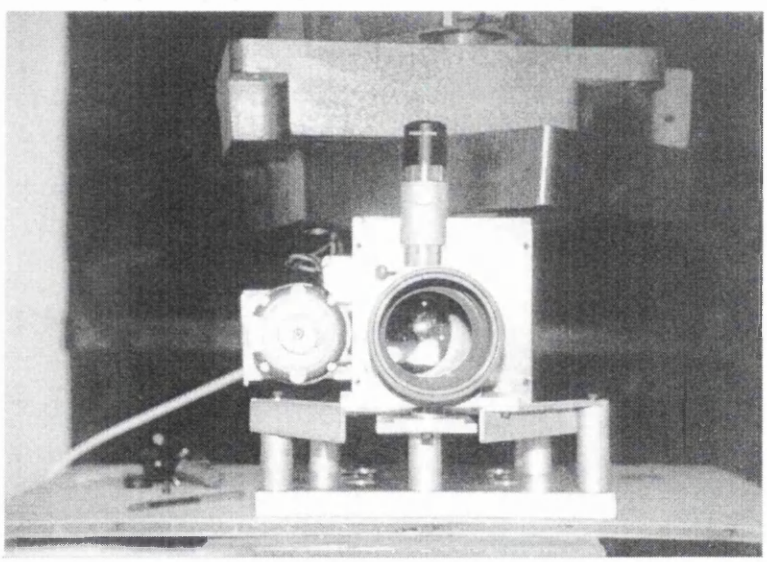

Fig. 5.1. The CCD-Polarimeter is shown as used in the experiments in the laboratory.

5.1.2 First light (laboratory)

The first test modulator was a thick superachromatic half-waveplate, inserted into the rotatable cell, at an angle so that the light beam is deviated. An additional polaroid

was fixed just in front of the CCD camera. Now if the telescope receives light of a completely polarized star, the recorded image should show a $\cos(4\alpha)$ modulation (see Equation 3.18 on page 22) along the circumference of the ring image. After the telescope and the artificial star were aligned and the focus was adjusted, several exposures were acquired. Figure 5.2 on the following page shows an example. The four intensity peaks expected from the modulation along the circumference can clearly be seen.

Looking at the intensity profile along this circle reveals something interesting. The $\cos(4\alpha)$ modulation seems to have an overlaid $\cos(2\alpha)$ modulation (see Fig. 5.3).

This can be explained by realizing that because the superachromatic half-waveplate was used at an inclined angle, it acted as a partial polarizer. The intensities of the reflected and refracted components behave according to the well known Fresnel laws. An unpolarized beam may be resolved into $\parallel$ and $\perp$ components and their transmitted intensities are not the same, resulting in a partial polarization. A mathematical treatment is presented on page 41.

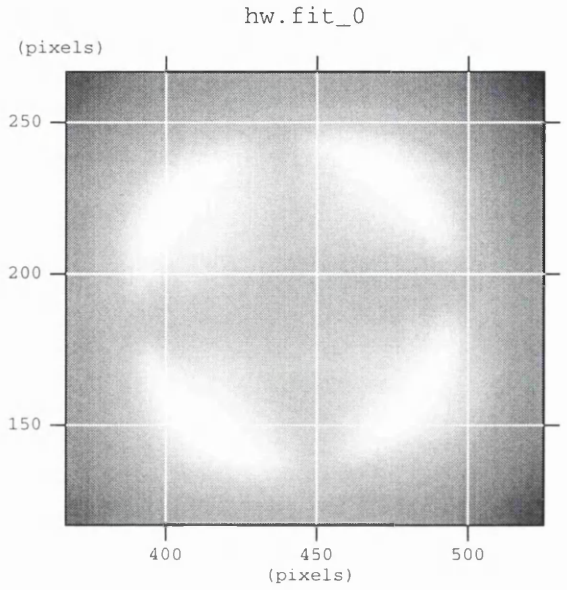

Fig. 5.2. The image of a 100% polarized light source is shown, taken with the half-waveplate version of the CCD-Polarimeter.

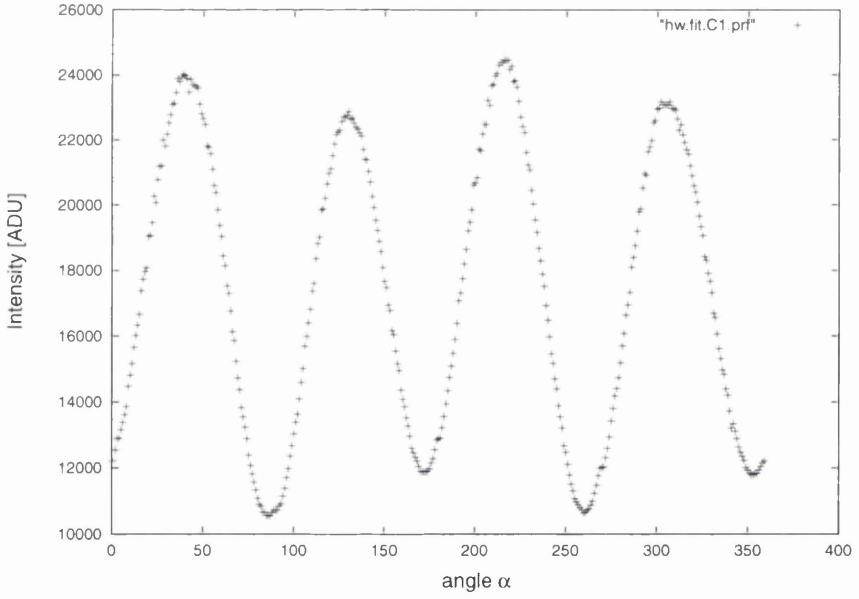

Fig. 5.3. The intensity distribution of Fig. 5.2 is shown. Apparently the expected $\cos(4\alpha)$ modulation seems to have an overlaid $\cos(2\alpha)$ modulation.

5.1.3 Mathematical derivation

To mathematically describe the situation, it is assumed that a partial polarizer is attached prior to the half-waveplate with its reference frame shifted by angle β compared to the reference frame of the half-waveplate. In terms of matrices the setup would be the following:

$$S^* = [\mathsf{P}]\,[\mathsf{R}(-\alpha)]\,[\Delta]\,[\mathsf{R}(-\beta)]\,[\mathsf{P}]_{K_{1,2}}\,[\mathsf{R}(\alpha+\beta)]\cdot S \tag{5.1}$$

To simplify the problem β is first assumed to be 0. For better readability the following abbreviations in the matrix for the partial polarizer $[\mathsf{P}]_{K_{1,2}}$ (see Table A.1) will be made:

$$K_+ = (K_1 + K_2) \qquad K_- = (K_1 - K_2) \qquad K_{12} = 2(K_1K_2)^{\frac{1}{2}}$$

$$\begin{bmatrix} I^* \\ Q^* \\ U^* \\ V^* \end{bmatrix} = [\mathsf{P}]\,[\mathsf{R}(-\alpha)]\,[\Delta]\,\frac{1}{2}\begin{bmatrix} K_+ & K_- & 0 & 0 \\ K_- & K_+ & 0 & 0 \\ 0 & 0 & K_{12} & 0 \\ 0 & 0 & 0 & K_{12} \end{bmatrix}\begin{bmatrix} 1 & 0 & 0 & 0 \\ 0 & \cos(2\alpha) & \sin(2\alpha) & 0 \\ 0 & -\sin(2\alpha) & \cos(2\alpha) & 0 \\ 0 & 0 & 0 & 1 \end{bmatrix}\begin{bmatrix} I \\ Q \\ U \\ V \end{bmatrix}$$

$$\begin{bmatrix} I^* \\ Q^* \\ U^* \\ V^* \end{bmatrix} = \frac{1}{2}[\mathsf{P}]\,[\mathsf{R}(-\alpha)]\begin{bmatrix} 1 & 0 & 0 & 0 \\ 0 & 1 & 0 & 0 \\ 0 & 0 & \cos\Delta & \sin\Delta \\ 0 & 0 & -\sin\Delta & \cos\Delta \end{bmatrix}\begin{bmatrix} K_+I + K_-(Q\cos(2\alpha) + U\sin(2\alpha)) \\ K_-I + K_+(Q\cos(2\alpha) + U\sin(2\alpha)) \\ K_{12}(-Q\sin(2\alpha) + U\cos(2\alpha)) \\ K_{12}V \end{bmatrix}$$

Assuming no circular polarization ($V = 0$):

$$\begin{bmatrix} I^* \\ Q^* \\ U^* \\ V^* \end{bmatrix} = \frac{1}{2}[\mathsf{P}]\begin{bmatrix} 1 & 0 & 0 & 0 \\ 0 & \cos(-2\alpha) & \sin(-2\alpha) & 0 \\ 0 & -\sin(-2\alpha) & \cos(-2\alpha) & 0 \\ 0 & 0 & 0 & 1 \end{bmatrix}\begin{bmatrix} K_+I + K_-(Q\cos(2\alpha) + U\sin(2\alpha)) \\ K_-I + K_+(Q\cos(2\alpha) + U\sin(2\alpha)) \\ \cos(\Delta)K_{12}(-Q\sin(2\alpha) + U\cos(2\alpha)) \\ -\sin(\Delta)K_{12}(-Q\sin(2\alpha) + U\cos(2\alpha)) \end{bmatrix}$$

To simplify the calculation, a reference axis can be chosen so that U is zero.

$$\begin{bmatrix} I^* \\ Q^* \\ U^* \\ V^* \end{bmatrix} = \frac{1}{4}\begin{bmatrix} 1 & 1 & 0 & 0 \\ 1 & 1 & 0 & 0 \\ 0 & 0 & 0 & 0 \\ 0 & 0 & 0 & 0 \end{bmatrix}\begin{bmatrix} K_+I + K_-Q\cos(2\alpha) \\ \cos(2\alpha)(K_-I + K_+Q\cos(2\alpha)) - \sin(2\alpha)(\cos(\Delta)K_{12}(-Q\sin(2\alpha))) \\ \cdots\cdots\cdots\cdots\cdots\cdots\cdots\cdots\cdots\cdots\cdots\cdots\cdots\cdots\cdots\cdots \\ \cdots\cdots\cdots\cdots\cdots\cdots\cdots\cdots\cdots\cdots\cdots\cdots\cdots\cdots\cdots\cdots \end{bmatrix}$$

The recorded intensity will be:

$$I^*(\alpha) = \frac{1}{4}\Big(K_+I + K_-Q\cos(2\alpha) + \cos(2\alpha)\big(K_-I + K_+Q\cos(2\alpha)\big) - \sin(2\alpha)\big(\cos(\Delta)K_{12}(-Q\sin(2\alpha))\big)\Big)$$

Since the half-waveplate is somewhat inclined, the light path is longer affecting the value of Δ being slightly larger than π, such that $\cos\Delta = -(1 - |\delta|)$.

$$I^*(\alpha) = \frac{1}{4}\Big(K_+I + (K_-Q + K_-IQ)\cos(2\alpha) + K_+Q\cos^2(2\alpha) - (1 - |\delta|)K_{12}Q\sin^2(2\alpha)\Big)$$

With constants $C_1 = K_+I$, $C_2 = K_-Q + K_-IQ$,
$C_3 = K_+Q$, $C_4 = K_{12}Q(1 - |\delta|)$:

$$I^*(\alpha) = \frac{1}{4}\Big(C_1 + C_2\cos(2\alpha) + C_3\cos^2(2\alpha) - C_4\sin^2(2\alpha)\Big)$$

Application of standard trigonometry leads to the following modulation:

$$\Longrightarrow I^*(\alpha) = \frac{1}{4}\Big(A + B\cos(2\alpha) + C_3\cos(4\alpha)\Big) \tag{5.2}$$

with

$$A = (C_1 + \frac{C_3 - C_4}{2}); \qquad B = (C_4 - \frac{C_3 - C_4}{2})$$

The record as shown in Fig. 5.3, however, shows that the predicted waveform is not an exact match. It can be made to do so by adding a phase to the harmonic as

would ensue if β does not have zero value, as would happen if the principal axes of the waveplate and the partial polarizer do not coincide.

Because of this complication this modulator was abandoned although in principal, a scheme could be designed to allow data reduction. Another modulator using a tilted glass plate (optical beam splitter) with a co-rotating polarizer was also tried in the laboratory (and on the telescope) but this was also abandoned because of disturbing ghost-images introduced by its coatings.

In the end the chosen modulator was in the form of a thin glass wedge (a laser anti-reflective device), but this was implemented at the time when the polarimeter was transferred to the Cochno observatory.

5.2 Real Stars

After several trials that mostly resulted in the insight that even more steel bars, screws and rubber is needed to reduce the persisting effect of vibration to an acceptable amount the system was finally ready, with the right glass-wedge, etc. All that was missing now, was a clear night.

On the evening/night of the 6th of April, 2000 we got our chance.

5.2.1 The objectives

It was planned to take several frames of an unpolarized star. The bright star α Leo (HD87901), also referred to as Regulus, was therefore a suitable choice. It was measured by Behr [1959] and is essentially unpolarized.

The primary objective of taking frames of an unpolarized light source is to check the system for polarization introduced by the telescope/system itself. Ideally the intensity profile along the circumference of the circular image should be flat, indicating that there is no instrumental polarization.

The secondary objective was to check if the squared pixels of the CCD chip are themselves sensitive to polarized light. Because the size of the pixels is small, being only a few times larger than the wavelength of light, some effects may be present and detectable. One notion is that the pixels might be more sensitive to light polarized in direction along the diagonal of the pixels than to light polarized parallel to the pixel-edges. If such effects are present, the intensity profile should show a $\cos(4\alpha)$ modulation because of the symmetry of the problem. Higher harmonics may also occur. If for example the direction of polarization is at an angle so that the 'slice' across the pixel has the length of an integer multiple of the wavelength, resonance effects are conceivable, similar to those occurring with diffraction gratings in the form of Wood's anomalies (see [Breckinridge, 1974]). This would be more apparent if the

wavelength pass band is sufficiently small. The current setup of the CCD-Polarimeter is an ideal experiment to check for this. Having a beam of unpolarized light entering the telescope, the rotating analyzer tube will polarize this light and produce a circular image on the CCD chip, with all possible polarization angles involved.

Further a series of frames will also be taken with a sheet polarizer placed in front of the telescope lens. The object of doing this is to check the system for its modulation efficiency. It also produces 'nice' pictures and intensity profiles according to Malus' law. Further these frames can be used to test the `analyze`-software.

Another interesting target would be to take some exposures of a star with known degree of polarization, to compare the results with already published values.

5.2.2 Data acquisition

The prototype CCD-Polarimeter was mounted onto the Grubb-Parsons 20-inch telescope in Cochno. This outpost of the Glasgow University Observatory is situated in the Kilpatrick Hills at an elevation of about 150m (500 ft), just far away enough to avoid Glasgow's light pollution. The 20-inch telescope serves merely to provide a platform for guiding and tracking of the prototype.

An IBM compatible laptop 486 computer, running under OS Win3.11, was connected to the HX-516 CCD camera. The software package PIX_H5 provided with the CCD camera was used to control the camera and store the data on the hard disk. "White" light was used for all exposures.

Flat fields

First, five flat-fields were acquired on the twilight sky at dusk. They were taken in exactly the same way as later the targets, with rotating analyzer tube. The integration

time was 120 seconds for each frame. Three dark frames with the same exposure time were also taken.

Regulus

As soon as it was dark, the telescope was pointed towards the bright star α Leo. First a dark frame of 60 seconds was acquired. Then the motor was switched on and ten exposures were taken with an integration time of 60 seconds. This was done using the PIX_H5 automode.

Artificially 100% polarized α Leo

A sheet polarizer was attached to the objective of the telescope, to artificially polarize the stellar light to 100%. Again two dark frames were taken first then five exposures of 120 seconds integration time respectively were taken via automode.

5.2.3 Data reduction

The first step on the way to calibrated frames is to convert the files to the FITS standard so that they can be processed further. Therefore the especially written program `fitconv` is used. This is necessary because the images saved by PIX_H5 fail in complying to the FITS standard (see Chapter 4.1). After the conversion, the raw images required calibration for CCD specific errors (see Section 2.3 on page 14). Several steps are required:

1) Correcting for Bias and Thermal noise

The raw images have to be corrected for bias and thermal noise. Therefore the dark frames that belong together are averaged. These averaged dark frames are then subtracted of both, the data frames and flat fields respectively.

2) Master flat field (MFF)

An MFF must be created. Therefore the dark subtracted flat fields are averaged and normalized. Unfortunately only three of the five flat fields could be used because the twilight sky was already too dark for the last two frames. According to Poisson statistics, the MFF has a relative uncertainty of about 0.5% for each pixel. Using more flat fields would reduce this contribution to the noise. For good statistical accuracy it would be preferable to have at least 20 frames. Fig. 5.4 shows the MFF for the current observations. Now, every data frame is divided by the MFF to correct for the non-uniformity of pixel sensitivity.

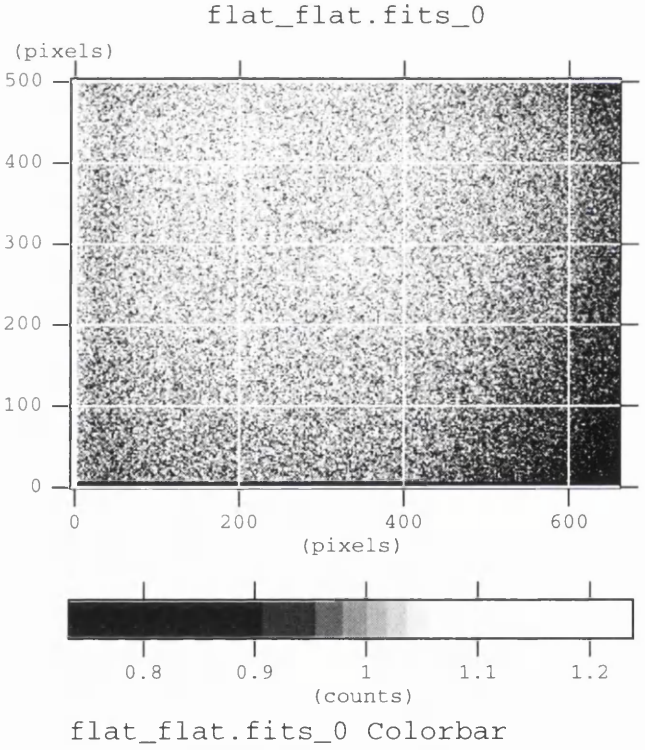

Fig. 5.4. The master flat field of the current observation is shown. It is noticeable that especially in the lower right corner of the pixel array the sensitivity is much smaller than in average.

For calibrating the raw frames, the image processing engine `eclipse` [Devillard, 1997] and the FITS utilities `ftools` provided by HEASARC have been used. Several C-Shell scripts were written to incorporate and automate the reduction procedures.

5.2.4 Analyzing the frames

Now the calibrated frames can be analyzed. The specially written software `analyze` (see Chapter 4) was used to determine the normalized Stokes Parameters q, u, the degree of polarization p and the intensity profiles along the circumference.

Regulus

The results for the frames acquired directly of the star α Leo are as follows:

TABLE 5.1: RESULTS OF α LEO

Frame	obs. time	q	Δq	u	Δu	p	Δp
1	21:44:52	0.0064	0.0002	−0.0003	0.0002	0.0064	0.0002
2	21:46:03	0.0100	0.0002	0.0042	0.0002	0.0109	0.0002
3	21:47:26	0.0095	0.0002	0.0011	0.0002	0.0096	0.0002
4	21:48:56	0.0104	0.0002	0.0039	0.0002	0.0111	0.0002
5	21:50:29	0.0084	0.0002	0.0047	0.0002	0.0097	0.0002
6	21:52:03	0.0083	0.0002	0.0009	0.0002	0.0083	0.0002
7	21:53:39	0.0092	0.0002	0.0035	0.0002	0.0098	0.0002
8	21:55:14	0.0115	0.0002	0.0023	0.0002	0.0118	0.0002
9	21:56:50	0.0068	0.0002	0.0027	0.0002	0.0073	0.0002
10	21:58:26	0.0091	0.0002	0.0009	0.0002	0.0091	0.0002
mean		0.0090	0.0015	0.0024	0.0016	0.0094	0.0016

The values for q, u and p vary from frame to frame with a dispersion significantly greater than expected by the estimation based on photon counting statistics. This

becomes even more evident if the points (q, u) and p are plotted against frame number. This is shown in Fig. 5.5 and Fig. 5.6 on the following page. It is noticeable that most of the points are in the first quadrant. Also there seems to be a persistent degree of polarization, with the mean value of p at 0.0094 ± 0.0016. The standard error of the real repeated measurements is considerably higher than the error due to photon statistics of the individual measurements. Other noises are obviously present. The read-out noise (RON) is according to Starlight-Xpress approximately 15 electrons RMS. A simple estimation, however, shows that the effect of the RON is largely smaller than the photon noise and is not responsible for the high scatter. Assume a CCD-pixel is holding 10000 photon-electrons. The relative error due to photon counting statistics would be $\pm 1\%$, the relative error due to the RON is only $\pm 0.2\%$; the latter can therefore be treated as insignificant.

Where is the instrumental polarization coming from?

By looking at the data two questions arise:

1) Is there really a non-zero polarization and if yes, where is it coming from?

2) Why do the values vary from frame to frame to such an extent?

To check for this, it is sensible to have a look at the actual data of the frames that were used to calculate the normalized Stokes parameters. Therefore it is useful to look at the intensity profile along the circumference of the circles. Figure 5.7 shows the profile of frame number 1. It may serve as an example for the others because it turned out that they all show similar features. It is noticeable that the profile shows neither a $\cos(2\alpha)$ modulation nor a straight line, but instead the intensity is varying asymmetrically with a minimum at around 100°. The dominant modulation is one of $\cos(\alpha)$, directly related to the mechanical rotation of the modulator. There must also be a small quantity of the harmonic $\cos(2\alpha)$ present which is detected as the

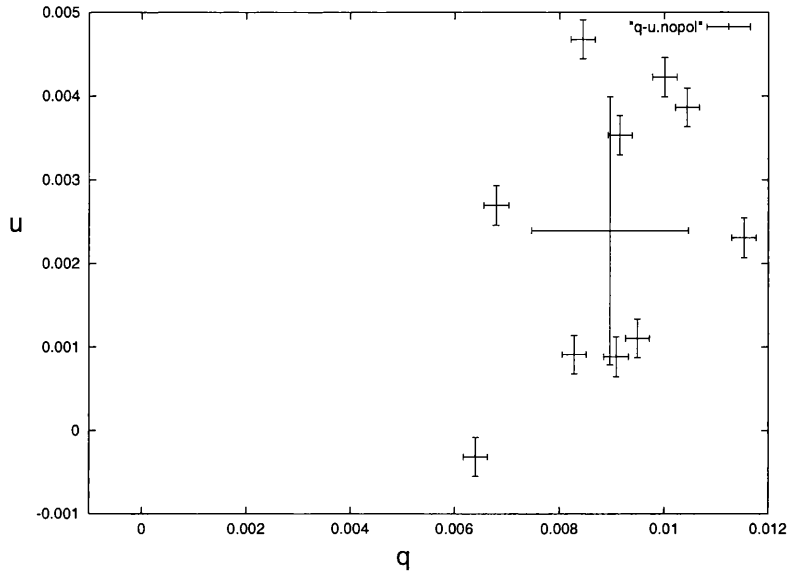

Fig. 5.5. $q - u$ plot of the test series with α Leo. The individual measurements are the points with small error bars representing the estimated photon noise. The point with the large error bars is the mean value.

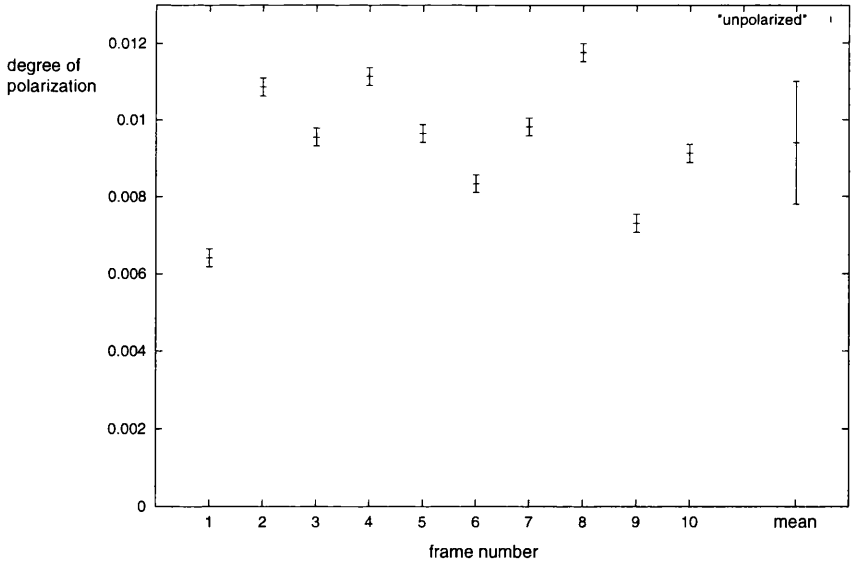

Fig. 5.6. The values for p of the test series with α Leo are plotted against frame number.

polarization being present. Small fluctuations of the intensity of ~5% over an interval of a few degrees are noticeable but do not show a repeated pattern. If the pixels are polarizationally sensitive to polarized light the effect is less than 5%. Probably these fluctuations are due to instrumental noise

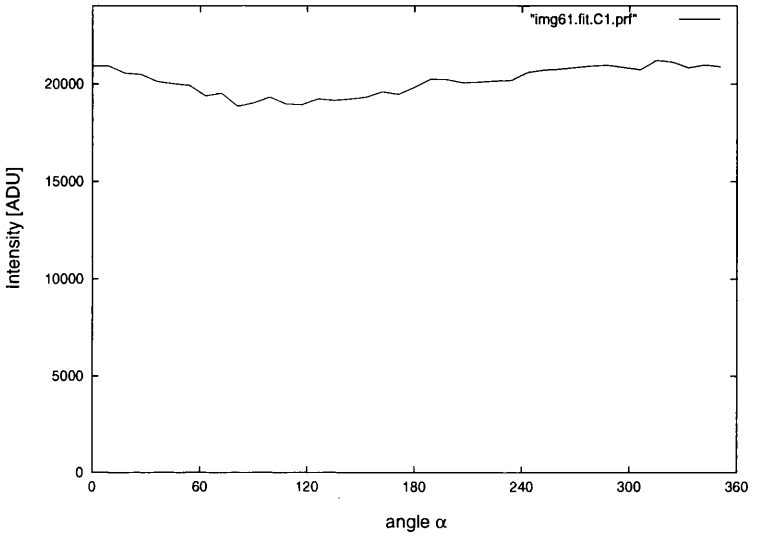

Fig. 5.7. Example for an intensity profile along the circular image of an unpolarized star.

There may be several possible reasons for this unfortunate profile. One possibility is that the motor did not run in a uniform way. There was a hint of this by listening to the motor's noise during observation. Maybe the tube rotated a little bit faster on a part of its revolution than on the average, resulting in an uneven intensity distribution as shown in Fig 5.7.

Another reason may be inaccurate flat fielding. Since only three frames could be used to generate the MFF, the statistical value of it is very poor. It could be that the sensitivity of the pixels is varying over the area where the circle is imaged and that the flat fielding was too poor to calibrate the frames properly.

It might be also that the flat fields have not been illuminated uniformly. This would introduce artificial fluctuations of the intensity values that are not spatially random — in contrary to the fluctuations due to photon counting statistics. These noise patterns would certainly have relevance to the intensity distribution of the ring and could introduce a spurious polarization signal.

Imprecise alignment of the telescope could have led to the light being spread unevenly along the circle. Parts of the resulting ring could be thicker than others. In this case and if not the maximum thickness of the ring is considered for the analysis, photons will be 'lost'. This may also have contributed to the poor profiles.

Having the profile in mind, the calculated degrees of polarization can be explained. The software does not care whether or not the profile shows a $\cos(2\alpha)$ modulation — it simply applies its algorithm (see Section 4.2.3) and performs the calculations. The algorithm is designed to concentrate on the $\cos(2\alpha)$ modulation and filter out the odd harmonics including the fundamental. But in these profiles, the fundamental harmonic is not a clear $\cos(\alpha)$ and in this way polluting the results. This problem could be avoided by either changing the algorithm, for example fitting a $\cos(2\alpha)$ curve to the profile and use this fit to calculate the normalized Stokes parameters, or adding a kind of quality check routine, that assesses the profile for symmetry and adjusts the errors where appropriate.

But since the goal is a high accuracy polarimeter, more effort needs to be applied to provide a uniform revolution of the analyzer tube without vibration. As mentioned earlier a MFF of higher quality would be desirable since it cannot be ruled out that incorrect flat fielding caused the unseemly intensity profile.

5.2.5 Regulus with polaroid

The results for the series of frames acquired with a sheet polarizer in front of the telescope are as follows:

TABLE 5.2: RESULTS OF ARTIFICIALLY 100% POLARIZED α LEO

Frame	obs. time	q	Δq	u	Δu	p	Δp
1	22:08:40	0.3455	0.0003	0.9193	0.0005	0.9821	0.0005
2	22:10:36	0.3671	0.0003	0.9124	0.0005	0.9835	0.0005
3	22:12:52	0.3733	0.0003	0.8886	0.0005	0.9638	0.0004
4	22:15:19	0.3506	0.0003	0.8685	0.0004	0.9366	0.0004
5	22:17:51	0.3489	0.0003	0.8293	0.0004	0.8997	0.0004
mean		0.36	0.01	0.88	0.03	0.95	0.02

In Fig. 5.8 the values of p are plotted against frame number. Looking at the results, especially those for p, it is evident that there is a trend with the values falling from frame to frame.

Only the first two values fairly match around 98.3 $\pm$0.1% — a little lower than the expected 100%. Unprecise subtraction of the background is probably the reason for this. It may also be a sign that the sheet polaroid is not 100% efficient over the whole spectrum. Measurements with different colour filters would be interesting, to examine the efficiency of the polaroid for different wavelengths.

But why are the values of p decreasing? One possibility to explain the continuous fall in the value of p is, that the background noise was steadily increasing during the run and that no allowance was made for this. A perfect intensity profile of the ring image of a 100% polarized light source should have a $\cos(2\alpha)$ form and go down to zero at the minima. If the background noise is not accurately corrected, the profile does

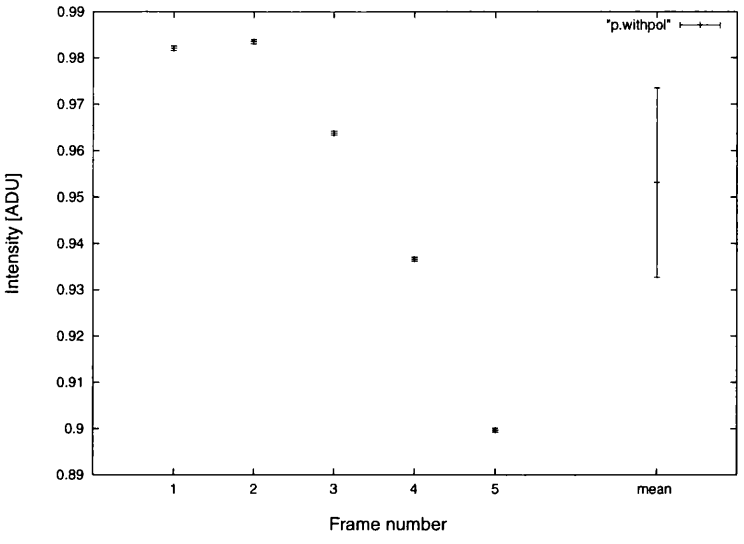

Fig. 5.8. 100 % polarized star — p plotted against frame number.

not reach zero in its minima. Hence the measured degree of polarization will be less than 100%.

To look for this, it might be interesting to plot the mean value of the data frames against frame number. If the background noise is rising for whatever reason, the mean value should rise as well (see Fig. 5.9 on the next page).

Fig. 5.9 clearly shows that a rising background level is the reason for the falling values of p. But what gave rise to the increasing background? One reason could be that the CCD chip was getting warmer during the run, thus increasing the thermal noise. Since the dark frames have only been taken before the series of exposures, they would not reflect the increased thermal noise of the later frames.

Another more spectacular and uncommon reason could be the following: Even from the dome environment it was obvious that the brightness of the sky was undergoing strange fluctuations. Using the automode to acquire the exposures, the "crew" left the telescope dome to have a look at the night sky. Instead of encountering the starry sky,

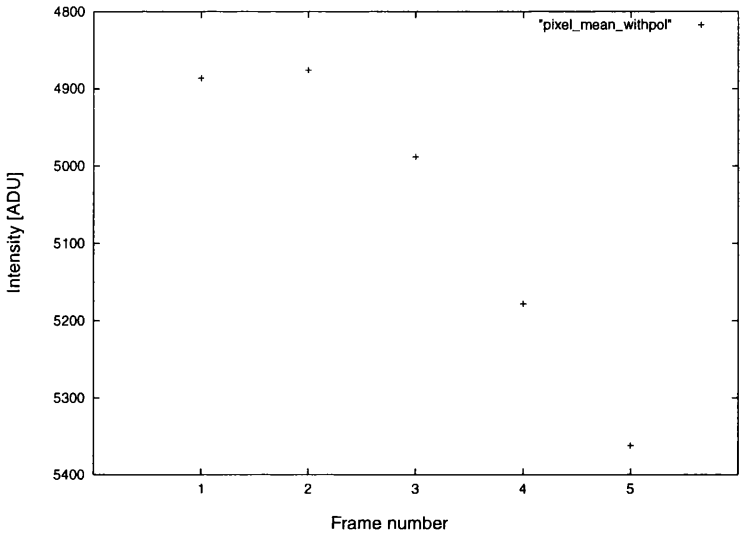

Fig. 5.9. 100 % polarized star — mean intensity value of the frame taken over its complete area is plotted against frame number. Note that the scale of the ordinate is inverted so that the trend is more readily compared with Fig. 5.8. The points follow exactly the same trend as the values for p in Fig. 5.8.

decorated with a few clouds, a beautiful apparition of an Aurora Borealis had commenced and within minutes painted the sky in its famous colours of excited elements. Some photographic pictures have been taken by the author and can be found in the Internet [Neumayer, 2000]. It is almost certain that the display of the Northern Light contributed significantly to the rise of the background of the exposures, but to rule out the theory of the chip getting warmer, the mean value of the frames taken without polarizer were checked. They show no signs of the chip getting significantly warmer during the series of exposures.

Unfortunately no exposures could be taken of a star with known degree of polarization, because the aurora would certainly disturb the quality of the frames. So the rest of the night was spent watching the natural spectacle.

6

Discussion and Conclusion

A new design for a CCD-Polarimeter has been presented. Based on Treanor's "Ring-Polarimeter" it combines the benefits of a modulating device, as usually employed in photo electric devices, together with the advantages of a CCD-Chip as imaging device.

In the final version, a rotating polaroid was used to modulate the light and a glass wedge was used to deviate the beam on a circle. Mathematical treatment of the setup shows that the rotating polaroid should modulate the intensity of incoming light by $\cos(2\alpha)$. A formalism is presented to calculate the normalized Stokes parameters from the received signal.

The new design carried some challenges for the data reduction. Because of the unique images, circles instead of point-like stars, no standard software could be used for the data reduction process. Special algorithms have been developed to locate these circles on the image array and to extract the polarimetric information, encoded as an intensity variation along the circumference.

Although the presented algorithms worked fine, additional functions to analyze the data would be useful. A weak point of the algorithm is that it can not determine the center of 100% polarized rings with their minima lying either on the same row or column. Additional scans along the diagonals would help to circumvent this problem

and would enhance the accuracy of the center position. Further it would allow a better judgement of the ring's shape. Elliptical rings for example would hint on misalignment of the telescope setup.

A bread-board designed prototype has been built, mainly of second hand parts. Tests in both the laboratory and at the observatory have been carried out. During these tests several weaknesses of the design emerged. The 'transfer-lens' incorporated to reimage the focus on the CCD chip and mounted on an optical bench inside the box was difficult to access and hard to adjust in a precise way. Mounting of the lens on a gear rack, ideally accessible from outside the box, would greatly simplify the focusing process. But the main problems affecting all the tests and development were with the motor. Vibrations were generated which could only be reduced to an acceptable amount by using additional steel bars and damping material to stabilize the system. Mounting the motor on the base-plate and independent of the instrument-box could further improve the stability of the CCD-Polarimeter. Another problem was that the analyzer tube was probably not rotating in a uniform way. Hints that this was happening were suggested by variations in tone in the audible noise. Friction in the gear wheels, the ball-race and the quality of the motor might be reasons for this. It would be interesting to monitor the rotation by means of a tachometer. The ideal drive for the analyzer-cell would be the use of a hollow-shafted motor with the modulating and deviating optics housed inside.

After the period of testing and improving of the CCD-Polarimeter, the unpolarized star α Leo was measured. Ten exposures were taken and the normalized Stokes parameters were calculated. The mean value for p was 0.009 $\pm$0.002, the ascribed uncertainty giving a preliminary indicator of the potential of the method for accurate bright star polarimetry. It may be noted that the error is larger than anticipated and further experiments should be able to identify the problems and allow them to be removed. However, this apparent degree of polarization may not be ascribed to α Leo; a closer

look to the obtained data revealed that a spurious signal dominated the records. Again further improvements of the instrument would be necessary.

The frames of α Leo were also interesting as they allow an investigation as to whether the pixels are themselves sensitive to polarized light. As the modulator spins, the annulus on to which the 100% polarized radiation falls on the CCD receives a direction of vibration which depends on the phase of the rotation. The intensity profiles along the circumferences of the obtained circles showed small fluctuations $\sim<5\%$ of the intensity over small sections. These patterns of fluctuations, however, did not repeat with a $\cos(4\alpha)$ modulation and cannot be ascribed to the pixels being polarizationally sensitive. The fluctuations may well arise from inadequate calibration by the flat-fielding process. It appears likely that any polarizational sensitivity of the CCD pixels is less than 1%.

Several exposures of α Leo were taken with a sheet polarizer attached to the telescope lens. Only the first two frames could be used for the calculation of p, the later exposures were disturbed by fluctuations in sky background caused by Northern Lights. A degree of polarization of 98.3 $\pm$0.1% was calculated — a little lower than the expected 100%. This could signify that the polaroid is not 100% efficient over the spectral range involved with the experiments. It might also result from unprecise subtraction of the background.

Because of bad weather conditions and other time constraints no further observations were carried out. Measurements of stars with known degree of polarization would be desirable. This would allow to compare the results of the observation with already published values and hence would be a test for the accuracy of the instrument. Also it would be interesting to use the instrument as a field-polarimeter. With an appropriate deviation angle, the bright stars of the Pleiades, for example, could be measured simultaneously.

The tests with the CCD-Polarimeter have shown that once the mechanical problems are overcome, this design represents a potential technique to measure the Stokes parameters of stellar light. Theoretically an accuracy for p of $\pm 7 \times 10^{-5}$ could be achieved with one single exposure.

The ultimate design would have a hollow-shafted motor as drive for the modulator. A plane-parallel, anti reflective glass plate with adjustable inclination angle would be ideal to deviate the light. It would allow choice of the appropriate deviation angle, whether a large field is to be studied simultaneously, or single stars are to be measured with high precision.

Rather than being stand-alone equipment, the module could also be designed for attachment to a conventional telescope allowing fainter stars or star-fields to be investigated.

Appendix A

Theoretical Background

This chapter aims to give a brief introduction into the theory of polarized light and its measurement. The topics will be restricted to those necessary for the understanding of the presented polarimeter. Most of the information is derived from Clarke and Grainger [1971].

A.1 Mathematical description of polarized light

To mathematically describe partially polarized light, it is convenient to split it into a completely polarized and an unpolarized component.

The polarized component of the beam of light can then be resolved again into its components along the x- and y- axis of a Cartesian frame:

$$E_x = E_{x_0} \cos(\omega t + \delta_x)$$
$$E_y = E_{y_0} \cos(\omega t + \delta_y)$$

with E_{x_0}, E_{y_0} as the amplitudes and δ_x, δ_y the phases of the x and y vibrations. The angular frequency is ω.

The equation of the polarization ellipse is obtained by eliminating t from the two equations and can be written as:

$$\frac{{E_x}^2}{{E_{x_0}}^2} + \frac{{E_y}^2}{{E_{y_0}}^2} - \frac{2E_xE_y\cos(\delta_y - \delta_x)}{E_{x_0}E_{y_0}} = \sin^2(\delta_y - \delta_x) \tag{A.1}$$

A.1.1 The Stokes Parameters

A beam of partially polarized light can be described by the Stokes Parameter. In general the 4 Stokes parameter[1] I, Q, U, V are given by

$$\begin{aligned} I &= {E_{x_0}}^2 + {E_{y_0}}^2 \\ Q &= {E_{x_0}}^2 - {E_{y_0}}^2 \\ U &= 2E_{x_0}E_{y_0}\cos(\delta_y - \delta_x) \\ V &= 2E_{x_0}E_{y_0}\sin(\delta_y - \delta_x) \end{aligned}$$

Their relation to the geometric description of the polarization ellipse is as follows.

Intensity	$I = I$
Azimuth	$\frac{U}{Q} = \tan 2\zeta$
Shape	$\frac{\lvert V\rvert}{I} = \frac{2\eta}{1+\eta^2}$
Handedness	*sign of* V

Here, ζ denotes the angle between the x-axis and the ellipse major axis. The ratio between the minor and the major axes is given by η.

[1] Four parameters are always required to describe the polarization ellipse — corresponding physically to its size, shape, orientation of the major axis and sense of rotation of the electric vector

For unpolarized light it is easy to see, that the Q, U, and V parameters are all zero. Although over a short timescale involving only few cycles of the wave, a definite polarization ellipse exists, the Q, U, and V values of these instantaneous ellipses are symmetrically distributed about zero. And over any normal experimental time their time average will be zero. The two components of our partially polarized beam of light can then be represented by the following Stokes vectors:

Unpolarized component: $I_U, 0, 0, 0$
Polarized component: $I_P, Q, U, V.$

The *degree of polarization* is given by:

$$p = \frac{I_P}{I_U + I_P}$$

Or in terms of normalized Stokes parameters:

$$p = \sqrt{q^2 + u^2 + v^2}$$

$$\text{with} \quad q = \frac{Q}{I} \quad u = \frac{U}{I} \quad v = \frac{V}{I} \quad \text{and} \quad I = I_P + I_U$$

A.1.2 Optical elements

Optical elements such as a retarder can be represented by matrices. The effect of the optical element on an beam of light can be simply calculated by multiplying the input Stokes vector by this element matrix. This formalism is known as the *Mueller calculus*. The initial values of the Stokes vector are related to a reference frame and if an optical element is set so that its axes are at an angle α to this reference frame, the Stokes vector has to be converted to the axes of the element, by multiplying the vector by a rotation matrix. Table A.1 on the following page shows the matrix representation for several optical elements.

TABLE A.1: MATRIX NOTATION OF OPTICAL ELEMENTS

Operation	Matrix
Partial polarizer[2]	$[\mathsf{P}]_{K_{1,2}} = \frac{1}{2}\begin{bmatrix} (K_1+K_2) & (K_1-K_2) & 0 & 0 \\ (K_1-K_2) & (K_1+K_2) & 0 & 0 \\ 0 & 0 & 2(K_1K_2)^{\frac{1}{2}} & 0 \\ 0 & 0 & 0 & 2(K_1K_2)^{\frac{1}{2}} \end{bmatrix}$
Perfect polarizer	$[\mathsf{P}] = \frac{1}{2}\begin{bmatrix} 1 & 1 & 0 & 0 \\ 1 & 1 & 0 & 0 \\ 0 & 0 & 0 & 0 \\ 0 & 0 & 0 & 0 \end{bmatrix}$
Pure retarder[3]	$[\Delta] = \begin{bmatrix} 1 & 0 & 0 & 0 \\ 0 & 1 & 0 & 0 \\ 0 & 0 & \cos\Delta & \sin\Delta \\ 0 & 0 & -\sin\Delta & \cos\Delta \end{bmatrix}$
Rotation[4]	$[\mathsf{R}(\alpha)] = \begin{bmatrix} 1 & 0 & 0 & 0 \\ 0 & \cos(2\alpha) & \sin(2\alpha) & 0 \\ 0 & -\sin(2\alpha) & \cos(2\alpha) & 0 \\ 0 & 0 & 0 & 1 \end{bmatrix}$

[2] $K_{1,2}$ are the intensity transmission coefficient of the element to light perfectly polarized in the orthogonal directions 1 and 2. (It is usual to choose these directions such that $|K_1 - K_2|$ is maximized.)

[3] Δ is the differential retardation or retardance

[4] The rotation angle α is measured anticlockwise from the x-axis.

Appendix B

ANALYSE - the source code

In this section, parts of the sourcecode of the analyzing program are shown, particulary those that have been described in Chapter 4. Although the programing style maybe inconsistent and not very beautiful, they may serve as examples for the interested reader. The routines use several global variables like the parameters **range** and **flex** or the table cnt that contains the positions and radii of the circles. They are defined as follows:

```
// structures
struct peaks{
  int n;                              // # of entries
  float p[cmax], r[cmax];
};

struct center{
  int n;
  float x,y,rx,ry;
};
// global variables
int X=500,Y=660;                      // X rows, Y columns
int x=X,y=Y,average=0;
int d=8,range=5,bin=1,flex=13;        // parameters
float mult=1.2,rmult=0.1;
char * filename;
int profile[360],entries[360];
int numberCenters=0;                  // # of centers found
```

```
center cnt[cmax];                    // Table of centers
```

The main routine provides an additional array, int v[500][660], that will contain the intensity values of the image. The image in FITS format will be loaded by the `load` routine with the usage of the `CFITSIO` library:

```
int load(char * file, int v[][Y])
{
  int s=0;
  int *anynul;
  long firstel=1,nelements,naxes[2]={X,Y};
  char filefit[80]="";
  int *nulval;
  fitsfile *fptr;
  printf("reading file: %s",file);
  // CFITSIO ROUTINE
  ffopen(&fptr, file, READONLY,&s);
  nelements=naxes[0]*naxes[1];
  if(fits_read_img(fptr,TINT,firstel,nelements,nulval,v,anynul,&s))
    exit(0);
  ffclos(fptr,&s);
  fits_report_error(stderr,s);
  printf(" successful!\n");
  return(0);
}
```

Probably the most challenging part of the program was the finding of the circles in the data array. This is done by the following routines. The routine `scancol` is not shown since it is essentially the same as `scanrow`.

```
int scan(int v[][Y],center * cnt)
{
  int r,i,j,k,s,count=0;
  float rc,rr;
  int base=abs(int(average*mult));
  peaks *row= new peaks;
  peaks *col= new peaks;
```

```
  // init the table of centers cnt
  for(i=0;i<cmax;i++)
    {cnt[i].n=0;cnt[i].x=0;cnt[i].rx=0;cnt[i].y=0;cnt[i].ry=0;}

  cout << "scanning with base " << base << " ..." << endl;
  for(r=0;r<y;r++)
    {
      s=scanrow(r,base,row,v);                    // Scan row r.
      if((row->n)>=1) {                           // More than 1 center?
        for (j=0;j<row->n;j++){                   // Check every column
          rr=row->r[j];                           // that goes through
          scancol(int(row->p[j]),base,col,v);     // a center.
          for (k=0;k<(col->n);k++) {              // Centers found again?
            rc=col->r[k];
            if((col->p[k]>=(float)r-0.5)          // Center on row r?
               &&(col->p[k]<=(float)r+0.5)){
              if((rc>=rr-RW)&&(rc<=rr+RW)){       // the radii match?
                if((col->p[k]>=cnt[count].x+1)    // Already in table?
                   ||(col->p[k]<cnt[count].x-1))  // Add and count them
                  {printf(".");  count++;}        // for averaging.
                cnt[count].n++;cnt[count].x+=col->p[k];cnt[count].rx+=rc;
                cnt[count].y+=row->p[j];cnt[count].ry+=row->r[j];
    } } } } } }
  for(i=1;i<=count;i++){          // Averaging
    cnt[i].x/=cnt[i].n;           // the multiple counted
    cnt[i].rx/=cnt[i].n;          // centers.
    cnt[i].y/=cnt[i].n;
    cnt[i].ry/=cnt[i].n;
  }
  printCenters(count,cnt);
  delete row;
  delete col;
  return(count);
}
int scanrow(int row,int base,struct peaks * neur,int v[][Y])
{
  int count=0,i,iold=0,j;
  neur->n=0;

  for (i=d;i<x-d;i=i++)
    {
      if(v[i][row]>base)
        {
          for(j=1;j<=d;j++) //checking if d points on left & right are lower
```

```
            {
              if((v[i-j][row]<v[i][row])&&(v[i][row]>v[i+j][row]))
                ;
              else break;
            }
          if(j==d+1)  // PEAK bei i!!!
            {
              if (count>0)
                {
                  neur->p[count-1]=(float)(i+iold)/2;
                  //printf("Peak bei %f \n",neur->x);
                  neur->r[count-1]=(float)abs(i-iold)/2;
                  neur->n=count;
                  if (count==cmax)
                    {printf("\n CMAX erreicht\n");break;}
                }
              iold=i;
              count++;
            }
        }
    }
  return(0);
}
```

Once the circles are found, they can be analyzed. Therefore an intensity profile along their circumferences is generated. Two different methods have been applied, both consider a ring of a certain thickness. The first method is used to plot a profile (see Section 4.2.4), the second to determin the normalized Stokes parameters (see Section 4.2.3).

```
long int fillprofile(int circle,int v[][Y],int param)
{
  long int pixelcount=0;
  double q=0,dq=0,u=0,du=0,pi,p=0,dp=0;
  int alpha;
  int m=0,i,j,c,cc,w,av=0,radius=0,rad=0,radmax=0;
  int lb=0,ub=0,db=0,rb=0; //left,uppper,down & right bound
  // float r=0,a,b;
  int r=0,a,b;
```

```
radius=int((cnt[circle].rx+cnt[circle].ry)/2);
initprof();

switch(param)
  {
  case 1: // radial method
    for(w=0;w<360;w++){
  m=0;
  for(cc=-flex;cc<=flex;cc++){
    i=int((radius+cc)*sin(((2*M_PI)/360)*w))+int(cnt[circle].x);
    j=int((radius+cc)*cos(((2*M_PI)/360)*w))+int(cnt[circle].y);
    if(v[j][i]>m){m=v[j][i];radmax=radius+cc;}
  }
  for(c=-range;c<=range;c++){
    rad=radmax+c;
    i=int(rad*sin(((2*M_PI)/360)*w))+int(cnt[circle].x);
    j=int(rad*cos(((2*M_PI)/360)*w))+int(cnt[circle].y);
    profile[w]+=v[j][i];
    pixelcount++;
  }
    }
    break;
  case 2: // sector method
    lb=int(cnt[circle].x-radius-range);
    rb=int(cnt[circle].x+radius+range);
    ub=int(cnt[circle].y-radius-range);
    db=int(cnt[circle].y+radius+range);
    for(i=lb;i<=rb;i++)
  for(j=ub;j<=db;j++)
    {
      a=(i-int(cnt[circle].x));
      b=(j-int(cnt[circle].y));
      r=int(sqrt(pow(a,2)+pow(b,2)));
      if((r>=radius-range)
         &&(r<=radius+range)){
        alpha=int((360/(2*M_PI))*(atan2(b,a)+M_PI));
        profile[alpha]=v[j][i] + profile[alpha];
        pixelcount++;
      }
    }
    break;
  default:
    printf("DEFAULT\n");
    break;
```

```
    }
  return(pixelcount);
}
```

The following routine calculates the normalized Stokes parameters and the estimated errors due to photon counting statistics:

```
int detpol(int circle,int v[][Y])
{
  long int In,s1,s2,pixelcount=0;
  double q=0,dq=0,u=0,du=0,pi,p=0,dp=0;
  double G=0.75;
  int param=1;

  cout << "Radial (1) or Sector (2) method?";
  cin >> param;

  pixelcount=fillprofile(circle,v,param);

  In=sum(0,360,v);                    // sum(a,b,v) is a subroutine that
  s1=sum(0,90,v)+sum(180,270,v);      // returns the sum of profile[a..b]:
  s2=sum(45,135,v)+sum(225,315,v);// profile[a]+profile[a+1]+...+profile[b]

  q=double(M_PI*(0.5-(double(s2)/In)));
  u=double(M_PI*((double(s1)/In)-0.5));
  p=double(sqrt(pow(q,2)+pow(u,2)));
  dq=(1/sqrt(G))*double(sqrt(pow((M_PI*sqrt(double(s2))/double(In)),2)+
    pow((M_PI*double(s2)/(double(In)*In)*sqrt(In)),2)));
  du=(1/sqrt(G))*double(sqrt(pow((M_PI*sqrt(double(s1))/double(In)),2)+
    pow((M_PI*double(s1)/(double(In)*In)*sqrt(In)),2)));
  dp=(1/sqrt(G))*double(sqrt((1/(q*q+u*u))*(q*q*dq*dq+u*u*du*du)));
  printf("-------------------------------------------------------------------\n");
  printf("I=%i, S1=%i, S2=%i\n",In,s1,s2);
  printf("q=%g +- %g\n",q,dq);
  printf("u=%g +- %g\n",u,du);
  printf("p=%g +- %g\n",p,dp);
  printf("total pixels used: %i\n",pixelcount);
  printf("-------------------------------------------------------------------\n");
  return(0);
}
```

Bibliography

A. Behr. *Veröffentlichungen der Universitäts-Sternwarte zu Göttingen*, 126, 1959.

J. B. Breckinridge. Diffraction Grating Polarization. In *Planets, Stars and Nebulae - studied with photopolarimetry*, pages 232+. The University of Arizona Press, 1974.

S. Chandrasekhar. On the Radiative Equilibrium of a Stellar Atmosphere. X. *ApJ*, 103:351+, May 1946.

D. Clarke and J. F. Grainger. *Polarized light and Optical Measurement.* Pergamon Press Ltd., Oxford, first edition, 1971.

D. Clarke and J. Naghizadeh-Khouei. Polarimetry using CCD detectors. In *Sensors and their Applications VIII*, pages 303+. IOP Publishing Ltd, Sept. 1997.

M. Dacke, D.-E. Nilsson, E. J. Warrant, A. D. Blest, M. F. Land, and D. C. Carrol. Built-in polarizers form part of a compass organ in spiders. *Nature*, 401(6752):470–473, Sept. 1999.

L. J. Davis and J. L. Greenstein. The Polarization of Starlight by Aligned Dust Grains. *ApJ*, 114:206+, Sept. 1951.

N. Devillard. The eclipse software. *The messenger No 87*, March 1997. URL `http://www.eso.org/eclipse/`.

T. Geherls. *Planets, stars and nebulae - studied with photopolarimetry.* The University of Arizona Press, 1974.

J. S. Hall. A photoelectric polarimeter. *Astronomical Journal*, 54:39+, 1948.

J. S. Hall and A. H. Mikesell. Observations of polarized light from stars. *Astronomical Journal*, 54:187+, Sept. 1949.

W. A. Hiltner. Polarization of Light From Distant Stars by Interstellar Medium. *Science*, 109:165, 1949.

E.-L. Malus. *Théorie de la Double Réfraction de la Lumière dans les substances cristallisées.* Paris, 1810.

D. Neumayer. The Aurora of 6th April 2000 at Cochno, 2000. URL `http://www.moonshineArts.de`.

Y. Öhman. "Effects of Polarisation in the Spectrum of β Lyræ". *Nature*, page 534, 1934.

W. D. Pence. CFITSIO, v2.0: A New Full-Featured Data Interface. In *ASP Conf. Ser. 1999: Astronomical Data Analysis Software and Systems VIII*, volume 172, pages 487+, 1999. URL `http://monet.astro.uiuc.edu/adass98/Proceedings/pencewd/`.

T. Platt. Starlight X e-/adu specs, 2000. URL `http://www.starlight-xpress.co.uk/discus/`.

D. Ratledge. *The art and science of CCD astronomy.* Springer, 1997.

J. L. Rivera and B. E. Penprase. Finding Circumstellar Disks Using Polarization And Infrared Excesses. In *American Astronomical Society Meeting*, volume 195, pages 10914+, Dec. 1999.

H.-J. Röser and K. Meisenheimer. CCD photo-polarimetry of the jet of 3 C 273. *A&A*, 154:15–24, Jan. 1986.

B. G. Stewart. The Correlation Between Normalised Stokes Parameters in a Sinusoidally Modulated Intensity Polarimeter. *A&A*, 143:235+, Feb. 1985.

G. G. Stokes. On the compositions and resolution of streams of polarized light from different sources. *Trans. Cambridge Phil.Soc.*, 9, 1852.

P. F. Treanor. A new technique for stellar polarimetry. *Mon. Not. R. astr. Soc.*, 138: 325+, Mar. 1968.